Matériaux pour la Géologie de la Suisse

GEOPHYSIQUE
No 22

Publiés par la Commission Suisse de Géophysique
Organe de la Société Helvétique des Sciences Naturelles,
subventionnée par la Confédération

GEOTHERMAL MAP OF SWITZERLAND (HEAT FLOW DENSITY)

Carte géothermique de la Suisse
(flux de chaleur)

Geothermische Karte der Schweiz
(Wärmestromdichte)

PHILIPPE BODMER
LADISLAUS RYBACH

En Commission
chez Kümmerly & Frey, Geographischer Verlag, Berne
1984

Address of authors:

Dr. Philippe Bodmer
Prof. Dr. Ladislaus Rybach
Institut für Geophysik
ETH-Hönggerberg
CH-8093 Zürich
Switzerland

Printed in Switzerland by Paul Attinger S.A., Neuchâtel

Preface

The Geothermal Map of Switzerland is no. 10 of a series of geophysical maps on the scale of 1:500000. These maps aim at the representation of the main geophysical parameters and have been prepared and produced by the Swiss Geophysical Commission. The geothermal conditions in the subsurface of Switzerland are represented in the form of a heat flow density map. The terrestrial heat flow density at the surface is closely related to the temperature field at depth.

The temperature distribution in the subsurface is, besides its scientific significance, of great importance for various fields of practical application:

- for the construction of underground facilities (e.g. for storage or transportation)
- for the development and use of groundwater resources
- for the exploration of hydrocarbons
- for the search and development of geothermal energy
- for the disposal of radioactive waste in geological formations.

The compilation of the Geothermal Map of Switzerland resulted from a joint effort of the Swiss Geophysical Commission and the Swiss Federal Commission for the Utilisation of Geothermal Energy and Underground Heat Storage. The latter Commission was especially responsible for a systematic collection, evaluation and compilation of subsurface temperature data in Switzerland.

Most heat flow density (HFD) determinations have been performed in objects available for measurements ("opportunity holes", tunnels or adits). In this regard, the cooperation of numerous constructing firms, oil exploration companies, consulting bureaus and various cantonal and communal authorities must be acknowledged.

The HFD map of Switzerland reflects the status of knowledge as at the end of 1983. A few new values that diverge from the trends shown on the map could the isoline pattern considerably.

The data set of the Swiss HFD map (with the geographical coordinates of the sites) is now incorporated in the International Heat Flow Density Data Catalogue (World Data Center).

The HFD data density in Switzerland is among the highest in the world. Nonetheless, many new heat flow density determinations, especially in the Alps, are needed to delineate more precisely the terrestrial heat flow pattern of Switzerland. Detailed geothermal mapping in the scale of 1:100000 is presently in progress in northern Switzerland; the Heat Flow Density Map of Switzerland will serve as its starting base.

Thanks of financial support are due to the Swiss Federal Office of Education and Science, the Swiss Federal Office of Energy Economics, the Swiss National Science Foundation, the Swiss Academy of Natural Sciences, the Swiss Federal Institute of Technology and - last but not least - to the Swiss Federal Office of Topography for printing the first "Geothermal Map of Switzerland".

On behalf of the

Swiss Federal Commission for the Utilisation of Geothermal Energy and Underground Heat Storage

Ladislaus Rybach

Prof. Ladislaus Rybach
President

Swiss Geophysical Commission

Stephan Mueller

Prof. Stephan Mueller
President

December 1984

Summary

The geothermal conditions in the subsurface of Switzerland are represented in the form of a map of the terrestrial heat flow density on the scale of 1 : 500 000. The heat flow density (HFD, in mW/m^2) is the amount of heat flowing per unit time and area through the earth's surface from its interior. The HFD is closely related through the rock thermal conductivity distribution to the subsurface temperature field. Reliable information about the subsurface temperature distribution is of growing importance today for a variety of tasks including the planning and construction of subsurface facilities for either storage or transportation, the development and use of groundwater resources, the disposal of radioactive waste in geological formations, the exploration of hydrocarbons, and the search for and development of, geothermal energy.

The representation of HFD by isolines requires a certain minimum data density. The necessary data base has become available only in the past few years in Switzerland, despite of several pioneering achievements in geothermics made in this country a long time ago, including the first reliable measurement of the geothermal gradient (De la Rue & Marcet 1834) and the first HFD determination in continental Europe (Stapff 1883). In 1979, only nine HFD values had been reported. In the early 1980's, however, concentrated efforts of both the Swiss Geophysical Commission and the Swiss Federal Commission for the Utilization of Geothermal Energy and Underground Heat Storage resulted in numerous new HFD determinations. Thus, a data base of more than 150 values was available for the construction of the Swiss HFD map.

The HFD has been calculated as the product of the geothermal gradient (dT/dz) and the rock thermal conductivity K. In doing so, steadystate, one-dimensional conductive heat transfer was assumed. Measurement sites were omitted if the gradient was disturbed by moving groundwater. Both K and dT/dz can vary with locality. K depends mainly on the rock type and on petrophysical properties such as porosity. Because in most cases, no drillcores were available from the holes in which temperature was measured, a conductivity catalogue of the main Swiss rock types was established on the basis of laboratory K measurements. More than 300 samples were used for this. For all HFD sites, the thermal conductivity profile was obtained using the catalogue and the lithological profile of the drillhole. The Bullard-plot technique was then used to calculate the HFD.

Before calculating the HFD, corrections were applied to the temperature data. In addition to corrections for thermal disturbances caused by drilling fluid circulating within the drillholes, several other corrections related to conditions at the earth's surface were performed. These included corrections for temperature fluctuations (seasonal or paleoclimatic), topographic relief, and geological processes such as uplift/erosion and subsidence/sedimentation. The influence of these corrections on the HFD pattern of Switzerland is demonstrated by a series of maps which accompany the text. For the HFD map at 1 : 500 000, only the topographic correction was applied according to common practice. The Swiss HFD map is, therefore, compatible with the HFD maps of other countries. Computer codes have been developed to perform all the necessary calculations.

The contouring of isolines at 10 mW/m^2 intervals was also done by computer. The geographical distribution of the data points used for contouring is highly uneven, being largely based on opportunity objects such as exploratory drillholes available for dT/dz determinations. Two-thirds of the HFD determinations have an uncertainty of $< 10\ mW/m^2$, one-fourth of 10 to 30 mW/m^2, and only a few percents of $> 30\ mW/m^2$. The different data classes are indicated on the map. The mean HFD for Switzerland is 85 mW/m^2. The isoline pattern is based on the state of knowledge as at the end of 1983. A few additional data points, with HFD values deviating from the displayed trends, could considerably change the course of the isolines. Areas in which the HFD may be disturbed by deep groundwater circulation are marked on the HFD map.

The surface HFD is a complex signal comprising long-wavelength, regional variations of deep (crustal and lithospheric) HFD, and superimposed shallower, shorter-wavelength local HFD variations. In Switzerland, the mean regional HFD decreases towards the south from the Jura to the Central Alps and increases again in the south of the Central Alps. The several superimposed local anomalies can be attributed to deep groundwater circulation systems.

Although the data base of the Geothermal Map of Switzerland is among the highest in Europe, periodic updating on the basis of new HFD determinations will be indispensable.

Table of contents

List of Figures and Appendices

were deformed and metamorphosed during the Hercynian orogeny, and again during the Alpine event (partly also thrusted);
- the *Penninic*, lower and upper *Austroalpine units*, a complicated sequence of sedimentary, volcanic (ophiolites) and metamorphic (also basement-type) rocks of different age (Precambrian to Mesozoic), thrusted northwards during the Alpine orogeny. The degree of metamorphism in these units generally increases from north to south, where the units dip into a root zone;
- the *Southern Alps*, clearly separated from the rest of the Alps by the Insubric line, including the Ivrea Zone (ultrabasites and granulite facies metamorphic rocks of possibly Hercynian lower crust/upper mantle origin). In the north, crystalline basement units show a considerably lower degree of metamorphism (greenschist/amphibolite facies) than immediately north of the Insubric line. Further to the south, Mesozoic and Paleozoic sediments and thick Permian volcanics lie on this old basement. The units are derived from the same facies belt as the Austroalpine nappes.
  Directly adjacent to the Tonale line lies the Bergell granodiorite, an alpine granitoid.

The southernmost tip of Switzerland reaches into the Tertiary basin of the Po plain (Molasse of Como).

3. Data Base

The calculation of HFD requires a knowledge of both subsurface temperatures and the distribution of the rock thermal conductivity. Furthermore, in order to calculate the different temperature corrections, geological, hydrogeological, climatic and petrophysical information is also required (see chapter 4.).

3.1 Subsurface temperature data

Numerous geothermal data are available in Switzerland, mainly from drillholes in the northern foreland or from tunnels and shafts in the Alps. The quality of these data vary considerably, necessitating the elimination of unreliable data before interpretation is possible.

The different categories of temperature data used for mapping are discussed in the following sections. A list of all measurement points considered for further interpretation is given in **Appendix 1.**

3.1.1 Temperature Logs

With few exceptions, the temperature logs were measured by the Institute of Geophysics, ETH-Zurich, by means of a calibrated thermistor probe. All measurements were performed after sufficient equilibration time and hence represent the true formation temperatures.

This category includes the most reliable temperature data, because the borehole conditions at the time of measuring were known, and the measuring tool was carefully calibrated.

The shape of both temperature and differential temperature-depth profiles give information about the occurrence of water circulation in the vicinity of the borehole. An example is given in *Figure 1* (borehole Klingnau; at a depth of 210 to 240 m, a large cavity with considerable water losses was encountered during the drilling operation.

Where water movement is not parallel to the isotherms, heat transport due to convection is usually much more efficient than pure heat conduction. The identification of such convection zones is of primary interest in geothermal investigations.

Excluding the uppermost layers (Quarternary) and a few local disturbances the temperature-depth profiles in the Tertiary sediments of the Molasse basin are nearly linear. However, many local and regional temperature disturbances due to water or gas circulation can be detected within the Mesozoic sediments in the Molasse basin and along the Jura.

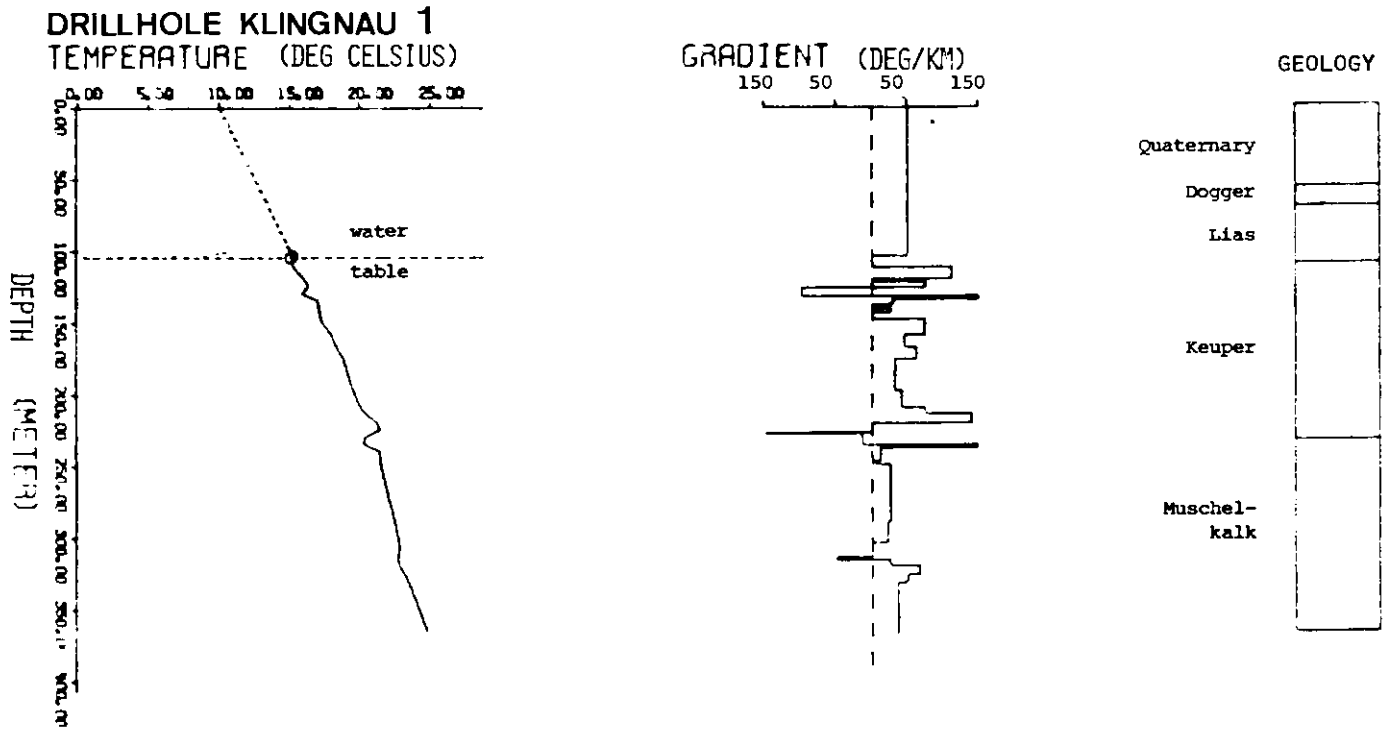

Figure 1: Example of a temperature log indicating water circulation in the vicinity of the drillhole.

3.1.2 Individual temperature values

Many individual temperature values from drillholes, tunnels and shafts have been published or documented in internal reports. A few data from formation tests also are available. Compared to the temperature logs their quality is much less reliable, because instrumental (e.g. calibration), hydrogeological or other disturbances are unknown and often difficult to assess. Many doubtful measurements have been eliminated; nonetheless this category should be considered with caution.

Usually the general trend of the temperature-depth curves is non-linear due to variations in thermal conductivity with depth, water convection, and the thermal history of the subsurface.
Temperature estimates between the measured points therefore, should not be evaluated by linear interpolation. A reasonable estimate of temperatures within lacking sections can be found by the use of master-curves (STEGENA, 1976). These curves are constructed on the basis of the best measured data within the area and are supposed to be representative for the regional geothermal field. For a typical set of curves for Switzerland see SYNTHESE (1982). Such estimations should not be used for detailed calculations, because they do not take into account temperature gradient changes due to local conductivity variations or water movement.

3.1.3 Bottom hole temperatures (BHT)

During borehole logging operations in deep boreholes, maximum thermometers are usually carried along with the different logging tools. The maximum temperature obtained is generally considered to be the "bottom hole temperature" (BHT), since in most cases, the temperature increases with depth. Because the measurements are usually performed a short time after the end of mud circulation in the borehole, these BHT values do not represent the true formation conditions. Rig time is too expensive, however, to perform BHT measurements after thermal equilibrium has been attained in the drillhole. Many BHT measurements were kindly made available by the Swiss petroleum industry.

A correction method for the disturbed BHT values was proposed by LACHENBRUCH & BREWER (1959). This method has been applied successfully in many cases, especially because the input parameters for the correction can usually be reconstructed from the drilling reports after completion of the holes.

The calculation of the correction requires several temperature observations (Tg) at the same depth at different times after the end of circulation (dt). Furthermore, the duration of the water or mud circulation at the bottom (tk) must be entered into the calculation. The equilibrium temperature of the formation (To) is obtained by plotting the Tg values versus log (tk/dt+1) and, as shown in *Figure 2*, by extrapolating the best-fit regression line towards the left hand side of the plot, corresponding to infinite equilibrium time (dt). The corrected temperatures can be treated analogously to the individual values mentioned in chapter 3.1.2.

There are two important restrictions to the method:

- The measured temperatures do not plot along a straight line after short equilibrium times,
- using powerful drilling equipment, the mud temperature is often increased due to frictional effects. At shallow depths (≦ 500 m), the measured mud temperature is often higher than the formation temperature. Since the location of the maximum temperature measured in the borehole is no longer a function of the geothermal conditions, but of the drilling history, the quality of the corrected data is strongly affected.

In both cases more sophisticated correction methods are required for the evaluation of the true formation temperature.

Figure 3 shows a measured and a corrected temperature-depth plot for the TREYCOVAGNES I drillhole in Western Switzerland (KRUESI *et al.*, 1978b; RYBACH & BODMER, 1980). The temperature correction shifts the measured temperatures towards a linear temperature-depth curve, which is typical for many sites along the Molasse basin. This linearity is the result of low radioactive heat production, small variations of thermal conductivity with depth, and the absence of water movements.

3.1.4 Temperatures in tunnels and shafts

Numerous rock temperature measurements have been determined during the construction of tunnels and shafts in Switzerland. Most of these data appear in the literature or in reports. The quality of these data varies according to the measurement technique used. It is important that the data were obtained a short time after the tunneling operation, since air circulation during or after the construction can strongly affect the rock temperatures.

Most measurements were performed in 1 to 2 m deep, water-filled drillholes. *Figure 4* illustrates the measured temperatures along the new Gotthard tunnel (RYBACH *et al.*, 1982). The temperature distribution is strongly affected by the overlying topography, for which a correction must be applied (see chapter 4).

3.2. Thermal conductivity

3.2.1 Measuring Technique

The thermal conductivity measurements which use a transient method were carried out with a QTM^R apparatus. With this instrument, a line heat source in a probe is pressed against a planar surface of the sample and is heated at a constant rate. The increase of temperature at the centre of this source, which amounts to about 10 to 20 °C, is measured by a thermocouple and allows the determination of the thermal conductivity of the sample. The accuracy of the thermal

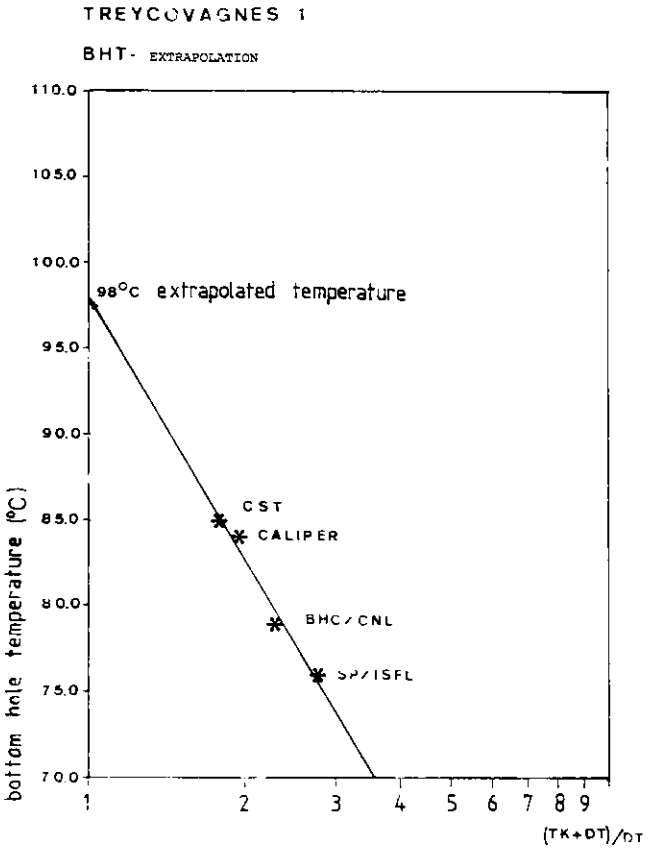

Figure 2: BHT-extrapolation (drillhole Treycovagnes I) from temperatures measured at different logging trips. Depth: 2395 m.

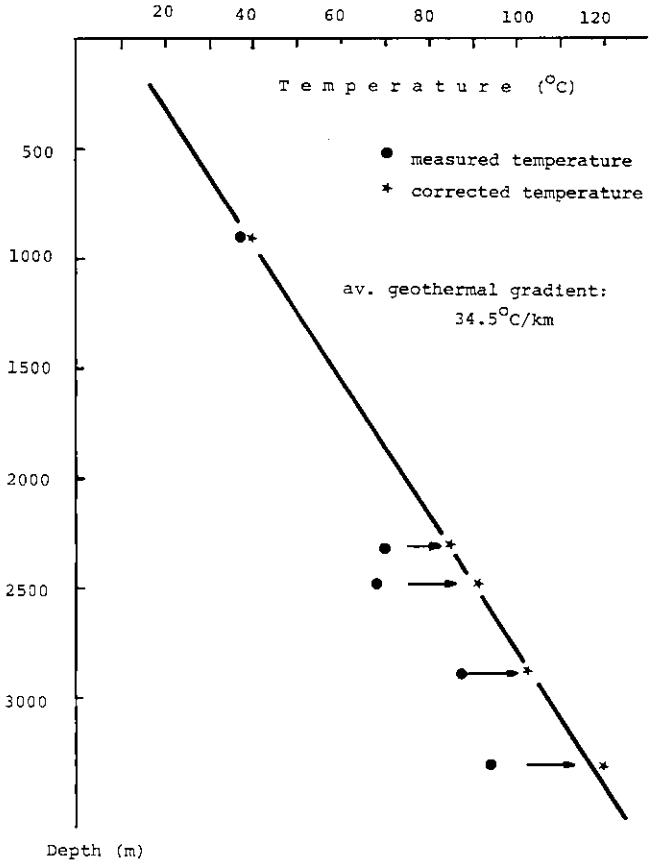

Figure 3: BHT corrections (drillhole Treycovagnes 1).

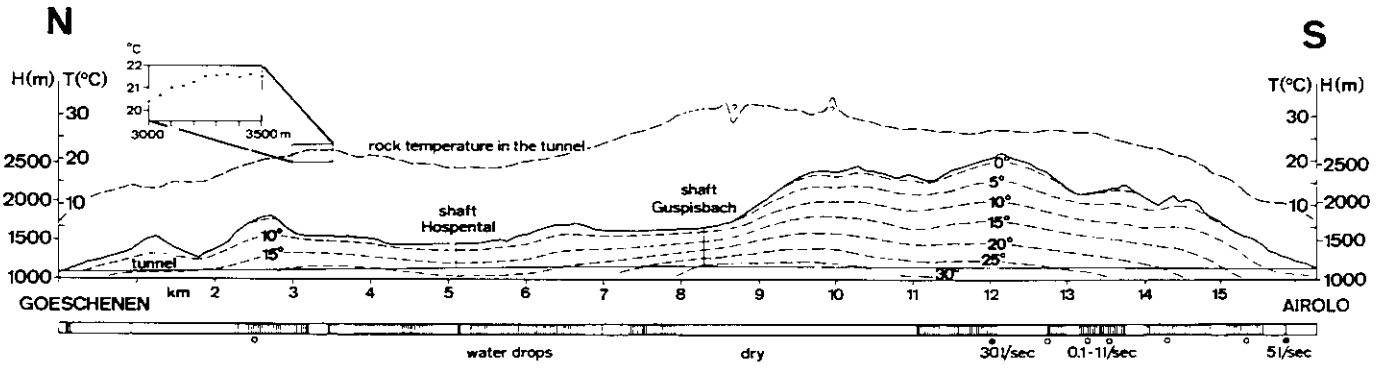

Figure 4: Temperatures along the Gotthard Road Tunnel. Measured rock temperatures (top), topographic profile with constructed isotherms and hydrologic conditions (bottom).

conductivity determination is approx. ± 5 %, the reproducibility ± 2 %. A thin foil covers the probe, avoiding penetration of water into the probe and enables the measurement of water saturated samples. The heating time is selected to be short enough to avoid thermal disturbances due to evaporation.

The thermal conductivity data obtained with this measuring technique originate from only a small rock-volume around the thermo-element. In order to avoid systematic errors due to the effect of inhomogeneities within the sample, the measurements have to be repeated at many different locations on the sample.

Both the measuring device and the technique are described in detail by SCHAERLI (1980).

For the determination of thermal anisotropy the measuring plane has to be cut perpendicularly to the layering or to the schistosity within the rock-sample. The thermal conductivity parallel to the layering ($K_{\parallel}$) can be determined directly by positioning the line source perpendicularly to this direction. In conjunction with a second measurement holding the line source parallel to the layers (K_{gs}), the component perpendicular to the layering ($K_{\perp}$) can be determined as follows:

$K_{\perp} = Kgs^2/K_{\parallel}$
(see also GRUBBE *et al.*, 1983)

In case of horizontal layering, in general, the information concerning $K_{\perp}$ is more important than $K_{\parallel}$, because it corresponds to the vertical component of thermal conductivity which determines the terrestrial heat flow. The anisotropy A is defined as the ratio $K_{\parallel}/K_{\perp}$.

The reliability of the QTM results is now generally accepted (see e.g. SASS *et al.*, 1983). Some intercomparison tests have been performed on Swiss samples covering the conductivity range in question by an absolute one-disk method. These measurements were performed by the Swiss Federal Institute of Material Testing (EMPA); a most satisfactory correspondence was found.

3.2.2 Rock sampling – results

In most drillholes selected for heat flow density determinations, no core samples were available for thermal conductivity measurements. For this reason, appropriate surface-rocks were sampled in order to obtain a representative conductivity profile across the geological sections found in the drillholes and also to establish a comprehensive thermal conductivity data catalogue of Swiss rocks (SCHAERLI, 1980; BODMER & SCHAERLI, 1980; SCHAERLI, 1983). Lateral E-W changes in lithology along the Alpine Foreland were partly taken into consideration by the construction of two schematic thermal conductivity profiles, one across the eastern part and one across the western part of the country.

Most samples encompassing the Mesozoic sediments were taken in drillholes or in outcrops along the Jura mountains, such that no information about possible N-S trends can be given. The thermal conductivity of the Tertiary sediments however, has been investigated in conjunction with the determination of other physical properties such as porosity, permeability, density etc. (SCHAERLI, 1980; SYNTHESE, 1982; BUECHI & BODMER, 1983). For this purpose, numerous drilling-cores and surface samples were collected in many locations, thus providing relatively accurate information about the spatial distribution of the physical rock properties. Reliable data on marls, claystones etc. are still missing.

Most samples used for thermal conductivity measurements were stored without protection, which would prevent the evaporation of the pore fluid. Therefore, these samples had to be resaturated prior to measuring. Except for rock-samples with very high porosity and permeability, it is recommended to evacuate the pore-volume before the rock material is watered. Only in one case, in the drillhole KKWB 7904 in Beznau, Northern Switzerland, could the cores containing their natural moisture be measured. The continuous core-profile, having a length of 317 m and covering the Mesozoic sediments from Dogger down to the Triassic, was sealed and evacuated immediately after the coring and cutting procedure (BODMER, 1980).

The results of the thermal conductivity determinations are tabulated in *Appendix 2*. Each value listed represents an average calculated from 5 to 30 single measurements on the same sample. The number of measurements taken was dependent on the degree of homogeneity of the rock material investigated.

The conductivity distribution along a schematic stratigraphic profile across the northern foreland of Switzerland is illustrated in *Figure 5*.

In both representations of the results, the thermal conductivities and their standard deviations are given both parallel and perpendicular to the layering (schistosity), along with the anisotropy.

3.2.3 Interpretation of the results

The thermal conductivity of a rock sample is strongly dependent on its porosity, on the shape of its pores and on the pore filling. In many cases these effects are even more important than the mineralogical composition of the sample.

A general dependency of thermal conductivity on the porosity was proposed by WALSH & DECKER (1966):

$$100 \log K_g = \Phi \log K_p + (100 - \Phi) \log K_m \quad \text{for } \Phi > 1\,\%$$

with K_g: measured thermal conductivity; K_p: thermal conductivity of the pore fluid: (air at 20 °C: 0.0257 W/m, °K, water at 20 °C: 0.599 W/m, °K); K_m:

thermal conductivity of the rock matrix; Φ: porosity in percent.

The thermal conductivity of water is approximately twenty times larger than that for air. Due to this large difference, the thermal conductivity determined on water saturated samples is higher than measurements on dry samples, even at very small porosities (SCHAERLI & RYBACH, 1984). *Figure 6* (top) illustrates the porosity effect on thermal conductivity on a rock with a matrix conductivity of 2.68 W/m, °K, the sample being water-saturated or dry. A comparison between theoretical and experimental data is shown (bottom): In most cases the measured values are in good agreement with the theory. Some experimental data on the diagram, however, are shifted to the left, indicating the occurrence of secondary porosity due to microfractures. These microfractures creating local inhomogeneities within the rock sample are better detected by the thermal conductivity measurement than by the porosity determination method (immersion technique); they are probably responsible for the systematic shift of the data.

The porosity dependence of the thermal conductivity is not negligible even at rock-porosities below one percent such as for crystalline rocks. Theoretical relations for low porosities were published by HASHIN & SHTRIKMANN (1962). According to the shape of the pores, one of the following formulae have to be selected (with $\beta = K_p/K_m$):

Maximum effect (isolated pores):

$$K_g = K_m \left[1 - \frac{3\Phi(1-\beta)}{2+\Phi+\beta} \right]$$

Minimum effect (interconnected pores):

$$K_g = K_m \left[1 - \frac{\Phi(1+2\beta)(1-\beta)}{\Phi(1-\beta)+3\beta} \right]$$

Numerous measurements on granite and gneiss samples with porosities between 0.4 and 1 percent showed dependencies according to the first formula (SCHAERLI & RYBACH, 1984).

Another relation which was investigated on core samples was the conductivity increase with depth as suggested by WERNER & FUCHS (1977), BALLING (1979) and others. This effect is primarily due to the rock compaction with increasing pressure and the alignment of clay minerals. The second effect is accompanied by an increase in anisotropy.

The general depth dependence after BALLING (1979) is estimated as follows:

$K(z) = 1.69 + 0.00068\ z$ (z being the depth in meters)

Only in very few cases could a depth dependence be observed. Generally this relationship is much more complex than described above, since the degree of compaction, which mainly creates the increase of thermal conductivity, depends strongly on the lithology. A very important effect is the alignment of elongated and/or flat minerals such as clay minerals, increasing the anisotropy.

Very strong nonlinear depth dependence of the physical rock properties within the uppermost 200 m below the earth's surface were observed and interpreted by BUECHI & BODMER (1983). These effects were observed on seismic data gathered in numerous exploration drillholes in Switzerland. The reasons for these non-linearities are probably episodic, reversible, and rapid changes of the groundwater level due to uplift and/or glaciation.

Table 1 shows the depth dependence of the thermal conductivity which could be observed on core material. Many other samples did not show any change of their properties with depth. These results suggest that, unless more detailed information is gathered, the depth dependence of the thermal conductivity cannot be taken into account properly for heat flow density determinations in Switzerland.

Table 1: Depth dependence of the thermal conductivity

DRILLHOLE/ formation	depth dependence	RK	N	depth range
TSCHUGG:				
Kreide/Malm	$K_\perp = 0.0029\ z + 1.1$	0.6	12	513–656 m
RUPPOLDSRIED:				
USM (Sandst.) – Malm	$K_\perp = 0.0010\ z + 1.6$	0.3	12	646–951 m
BEZNAU (7904):				
Opalinuston	$K_\perp = -0.013\ z + 2.0$	0.5	26	25– 64 m
Gipskeuper	$K_\perp = 0.042\ z - 2.5$	0.8	11	134–211 m
Opalinuston-Sulfatzone	$K_\parallel = 0.0074\ z + 2.0$	0.6	91	25–317 m
	$K_\perp = 0.011\ z + 1.2$	0.7	91	25–317 m

Legend:
$K_\parallel$, $K_\perp$: thermal conductivity parallel and perpendicular to the layering (W/m, °K)
RK: correlation coefficient
N: number of measurements
z: depth (m)

3.2.4 Selection of the thermal conductivity data for heat flow density determinations

For only a few HFD sites was the vertical distribution of the thermal conductivity measured in conjunction with the temperature log. In most cases the conductivity information was extrapolated from other drillholes or from corresponding rock material sampled at the surface. Using the thermal conductivity catalogue given in *Appendix 2*, the thermal conductivities were averaged by formation and attributed to the geological sections covered by the temperature measurements. *Figure 5* contains information about the average conductivity across several geological sections. These values can also be used for the interpretation of drillhole sites where the geological profile is not known in detail.

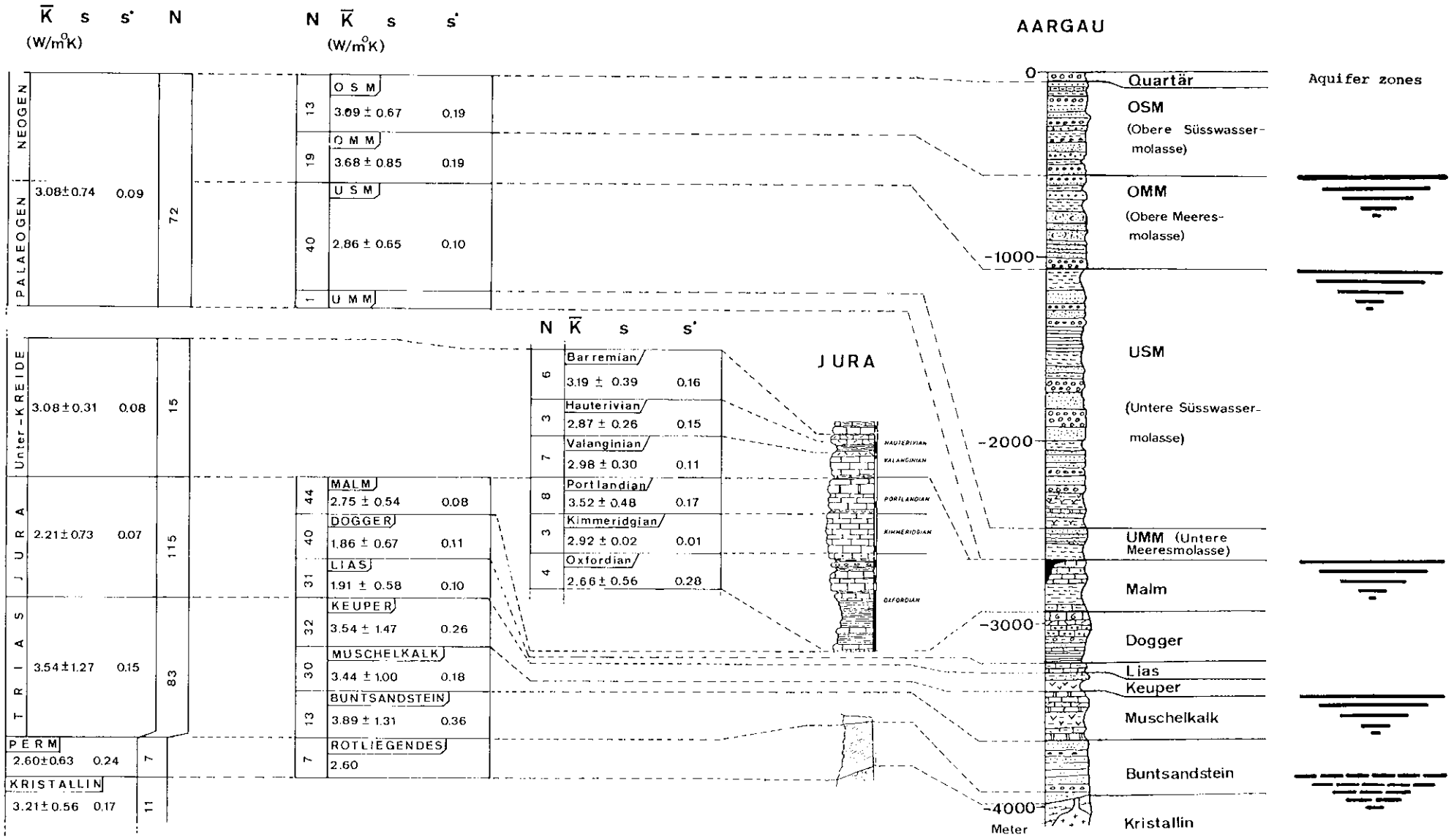

Legend: $\bar{K}$ = mean thermal conductivity (W/m°K)

s = standard deviation (single value)

N = number of samples measured

s* = standard deviation of the average value $\bar{K}$ $s' = s/(N)^{1/2}$

Figure 5: Thermal conductivity distribution along the stratigraphic column of the northern foreland in Switzerland.

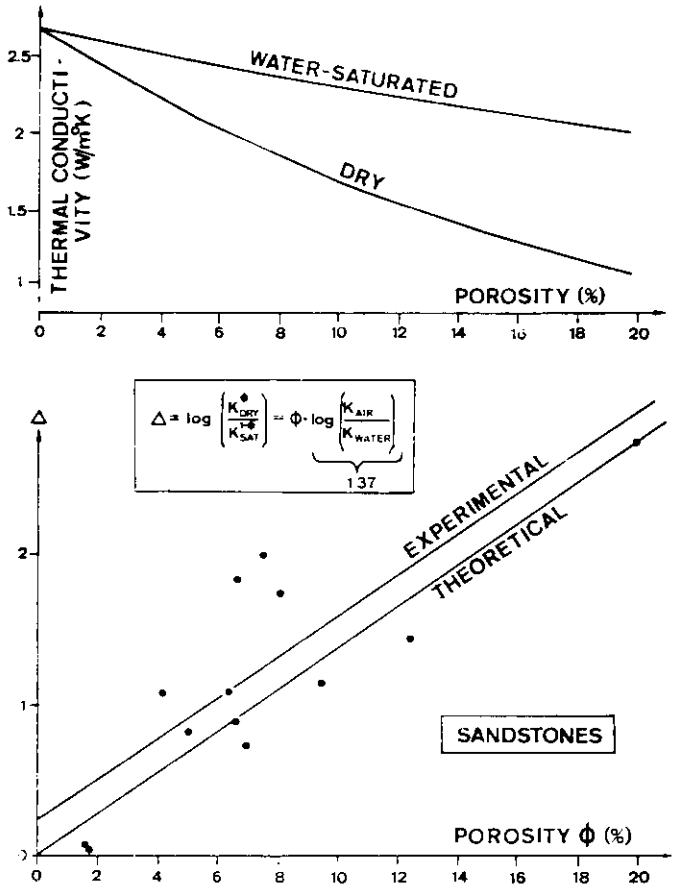

Figure 6: Effect of porosity on thermal conductivity of consolidated sediments. The dependency curves are significally different for dry and for water saturated samples.

The knowledge of the anisotropy permits the selection of the thermal conductivity component parallel to the heat flow. In most heat flow sites no exact information about the dip of the layering (i.e. from a dipmeter log) was available, such that horizontal layering had to be assumed. The error due to this assumption is negligible in most areas in the Northern Foreland of Switzerland. In the Alps and in the Folded Jura, however, this assumption is not valid, and the dip, therefore, has to be estimated from direct measurements in the field or at least from general trends in geological maps.

4. Temperature corrections

Depending on the purpose of geothermal mapping, different temperature corrections have to be applied to the measured data prior to the HFD determination. The corrections are of special importance in cases where the geothermal information has to be extrapolated in horizontal or in vertical direction. The most common corrections are the ones eliminating the effects of topography, paleoclimatic variations, uplift/erosion and subsidence/sedimentation. The topographic correction is a static correction which should be applied in any case, the other corrections, however, are only required for special applications of geothermal data.

Many different correction procedures have been published in the last decades. The desire to apply the correction technique which is the most suitable to the given regional geothermal conditions is often in contradiction with the necessity of adapting the calculated values to the format of other countries in order to enable the construction of maps on a continental or on a worldwide scale.

First attempts to establish international standard procedures in geothermics have been made by the International Heat Flow Commission and by the Commission of the European Communities (HAENEL, RYBACH & STEGENA, in prep.; BALLING *et al.*, 1981).

The different corrections to the geothermal gradient or to the temperature data are usually performed sequentially, correcting first for the most recent perturbation (BODMER & RYBACH, 1983). This procedure is inaccurate since the different disturbances, for which correction is necessary, took place during overlapping episodes; they should be treated simultaneously. A combined simultaneous calculation of the corrections is extremely arduous and the improvement of the results is in no relation compared to the increase of work and of computer time. Furthermore, it is generally impossible to obtain the requested base-parameters for detailed models.

The unknown proportion of conductive to convective heat transport represents a critical uncertainty in the correction of temperature data. Due to the lack of sufficient hydrogeological data, the convective heat flux can only be inaccurately estimated. In many cases the procedure is even inverted: the importance and the extent of water circulation systems is usually estimated by comparing the measured data after corrections (assuming pure conduction) with the expected temperature field. Large local anomalies in conjunction with pronounced variations in terrain-altitude suggest the occurrence of important convective processes. In an attempt to account for the topographic, erosional and paleoclimatic effects on the temperature field, the corrections have been applied to the subsurface temperatures rather than to the geothermal gradients. The main reason for this lies in the HFD determination technique used (cf. chapter 5) which uses temperature values. To perform temperature corrections on the Swiss data, especially the topographic correction, the use of a computer is necessary. The different steps during the correction procedure were interconnected in order to achieve the final results under minimum effort. Digitisation of the topography was unnecessary because of the prior existence of a digitised topography for Switzerland ("RIMINI-array"). This array covers the terrain with a meshwidth of 250 m (ZUEST, 1977; BODMER *et al.*, 1979).

A flow chart of the automatic correction procedure is illustrated in *Figures 7 + 8*. The first program (ASSEMB) reads all input-data related to the site under investigation, and especially the specifications of the corrections desired. The program itself then selects all parameters which were not specified in the input file

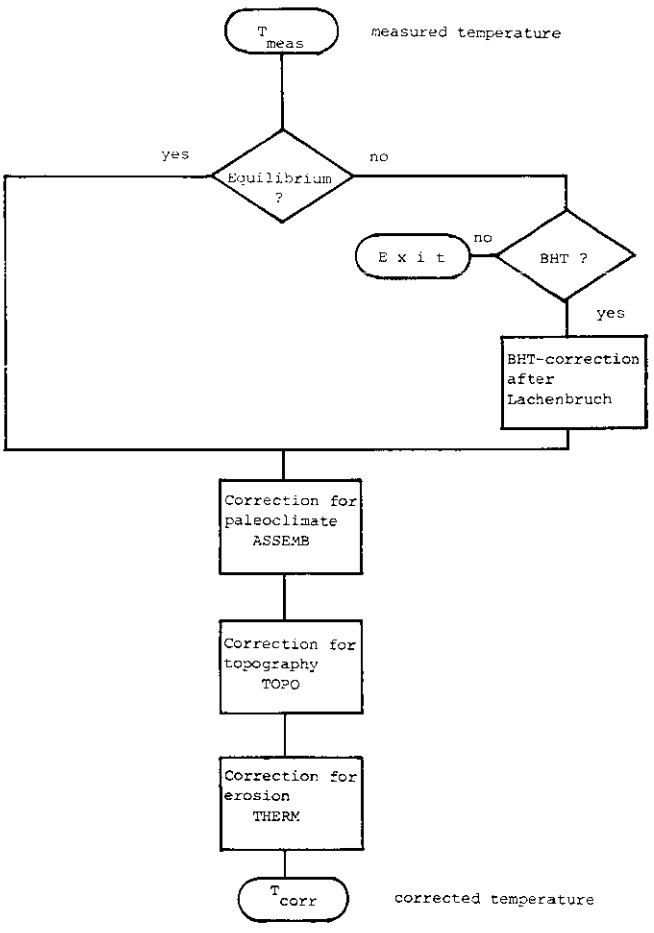

Figure 7: Flow chart for temperature corrections.

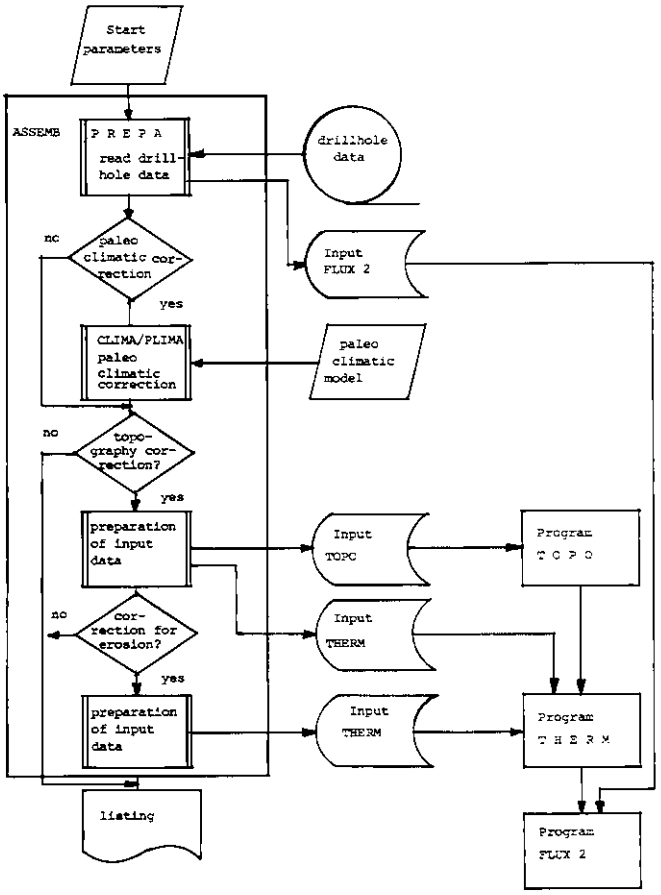

Figure 8: Flow chart for data processing with ASSEMB.

(= default values) and all parameters which are independent of the location of the heat flow site, i.e. the "geometric parameters" as defined in chapter 4.1.4 or by the paleoclimatic model of Switzerland (see chapter 4.3.3). Then ASSEMB assignes the data to the different correction programs or routines. These corrections are loaded automatically after completion of the initialisation routine.

The different correction procedures require the input of different data-files including the measured temperatures, the geological situation near the sites investigated, the corresponding distribution of the thermal conductivity etc. These data are stored on external files which are loaded automatically by the different programs or subroutines without special specification by the user, thus simplifying the data entry, especially for repeated interpretation for the same heat flow site.

The programs are designed for universal use with respect to the character of the heat flow site. Drillholes, tunnels, vertical or inclined shafts can be treated equally well, although the computation time can vary considerably according to the type selected, mainly due to the large size of the topography array required for horizontal data configurations (i.e. tunnels).

4.1 Topographic correction

4.1.1 Introduction

The topographic correction takes into account the distortion of the subsurface temperatures due to a relief surface.

Most methods assume a constant temperature or a given temperature distribution at the earth's surface and a constant heat flow at a lower boundary of the model configuration. The distorted isotherms are corrected assuming an idealised planar earth's surface (reference plane). This reference plane intersects the actual topography at the location of the site investigated as illustrated in *Figure 9*. Some correction methods can also take into account changes in topography (i.e. due to folding) or changes of surface temperature (due to uplift) with time.

The topographic corrections in Switzerland were performed according to the method of BIRCH (1950). This method, which accounts for a 3 dimensional, time-dependent topography was chosen among many others, because it can treat the terrain with a maximum degree of precision at a sufficient radius around the site investigated, with minimum computer memory and calculation time requirement. Correction techniques using a stationary topography (i.e. JEFFREYS, 1938) or 2-dimensional calculations are not accurate in areas such as the Alps. On the other hand, experience with detailed 3-dimensional models, such as finite element and finite difference models, has shown unfavourable

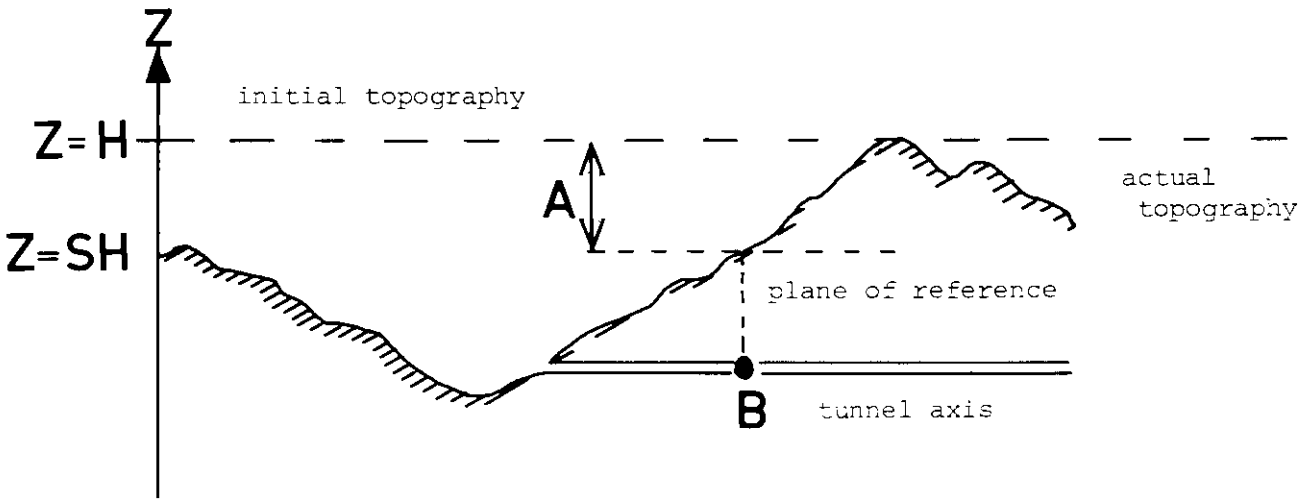

Figure 9: Definitions for topographic correction in a tunnel (TOPO and THERM).

results, since the simplifications required in order to reduce the computer memory will deteriorate the corrections.

The topographic correction dT_{TOPO} related to a reference plane (see *Figure 10*) is calculated as follows (BIRCH, 1950):

$$dT_{topo} = \frac{z}{2\pi} \int_0^\infty E(\beta) \frac{rdr}{R^3} \int_0^{2\pi} f(r, \varphi, t)\, d\varphi$$

where x, y, z are the coordinates of the measurement point; r and φ are polar coordinates on the reference plane; t the time of evolution of topography; f (r, φ, t) the change of the time-dependent temperature on present topographic surface;

$R = (r^2 + z^2)^{1/2}$

$E(\beta) = 2\text{erfc}(\beta) - 4i^2\,\text{erfc}(\beta)$

with $\beta = R/(4\chi t)^{1/2}$; χ: rock thermal diffusivity.

The numerical calculation of this formula is performed by the program TOPO. This program is a strongly modified version of the one described by ENGLAND (1976).

The reference plane, as illustrated in *Figure 10*, is divided into concentric rings within a maximum radius rmax. Each of these rings is subdivided into sectors with width $rd\varphi$ (see *Figure 10*) where the function f (r, φ, t) is determined.

It is important to note here that the topographic correction does not account for denudation but only for the change of shape of the earth's surface, departing from an initially planar topography.

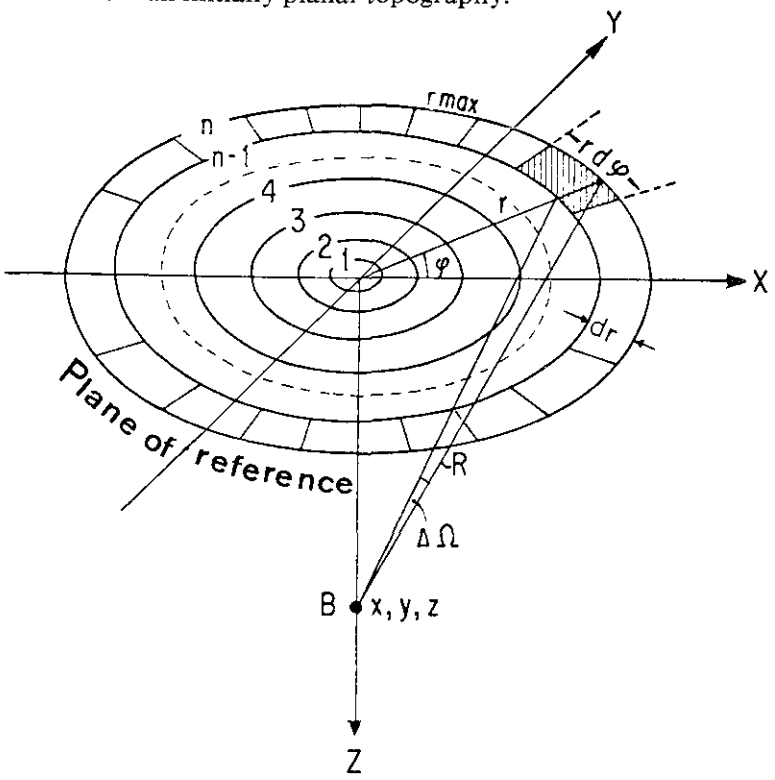

Figure 10: Geometric parameters for topographic correction.

4.1.2 Topography array "RIMINI"

The digitised topography of Switzerland ("RIMINI") was compiled by the Swiss Military Department. This file contains in sequential order 331 segments, each covering a sheet of the official 1 : 25 000 topographic map of Switzerland. Each segment is initialised by an identification header followed by the altitude data corresponding to a quadratic grid with a mesh width of 250 m. The data file contains the whole surface of the country plus small parts of the neighbouring countries.

The quality of RIMINI was tested prior to its application: Generally the error in altitude is less than 10 to 20 meters and the reliability of the file is thus acceptable for the topographic corrections. It should be noted, however, that major errors occur, especially in the Alps. Such errors have been detected in areas with very rugged topography, where the reading of the topographic map which was used for the digitisation became difficult. Furthermore, relative maxima in elevation (mountain peaks) are moved towards meshpoints in order to be fully covered by the grid. Many points outside the country were not digitised and therefore have the value zero.

The most negative feature of RIMINI, which may create significant errors in the temperature corrections, is that all areas which are covered by water are described by the altitude of the water surface, instead of by the effective topography at the bottom of the water.

4.1.3 Program TOPO

As described previously, the program TOPO calculates the topographic correction of subsurface temperatures measured in drill-holes, shafts or tunnels. First the program reads the input parameters as described in chapter 4.1.4. Then the subroutine HEIGHT is called in order to collect and to reassemble the terrain data around the site (RIMINI). The subroutine SURCLE calculates the mean value $\bar{f}$ for each ring. The value E (β) is calculated by FERFC and the integral across all rings (from r = 0 to r = ∞) is evaluated by DEPCOR. The area outside rmax is considered to have no relief and to have an altitude corresponding to the mean surface level within the topographic array defined. After the evaluation of the final correction for the temperature at one (tunnel) or several (drillhole) depths, TOPO prepares the output-files for the following processing step and the results are printed (see *Figure 11*).

4.1.4 Selection of the input parameters

Two input data categories have to be defined and entered into TOPO: the "geometric parameters" (usually defined by ASSEMB) and the "geological parameters" which also contain the climatic information (usually defined by the user).

The geometric parameters are strictly related to the correction technique and should have no influence on the final results.

A detailed sensitivity analysis was carried out by BODMER *et al.* (1979) according to which the values described in **Table 2** were recommended for selecting the geometric parameters.

Table 2: Selection of the geometric parameters for program TOPO

Symbol	Description	Optimum value*
rmax	max. radius of the digitized topography	4 km (Northern Foreland) 6 km (Alps)
dr	ring spacing	125 m
rd φ	width of sector within the rings	250 m

* in terms of accuracy and computer time

The geological and the climatic parameters have strong influence on the correction and, therefore, have to be selected carefully according to the conditions at the site investigated. This group of parameters includes the actual surface temperature, the atmospheric lapse rate, the initial geothermal gradient, the time of evolution of topography, and the average thermal diffusivity of the subsurface. The selection of these parameters was discussed more in detail by BODMER *et al.* (1979) and by BODMER (1982).

The climatic information, defined by the entry of the surface temperature and the atmospheric lapse rate (= free air gradient), can be evaluated from meteorological observations (i.e. ATLAS DER SCHWEIZ 1965). TOPO accounts for a differentiated entry of the free air gradients along N or S orientated slopes of the terrain.

The initial geothermal gradient Go which is assumed to be close to the corrected gradient is not known prior to a first evaluation of the terrain correction. In a first guess, it is assumed that the initial geothermal gradient is close to the value (Gm + Gf), where Gm represents the measured geothermal gradient, and Gf the atmospheric lapse rate. This assumption is correct in areas with small relief. Since the temperature correction is proportional to a (Go-Gf) (BIRCH, 1950), the gradient correction is also approximately proportional to this factor. A first run of TOPO using a guessed initial geothermal gradient Go in conjunction with the obtained resulting corrected gradient Gl allows the calculation of the proportionality-factor a:

$$a = (Gl - Gm)/(Go - Gf)$$

where $Go - Gf \ll Gl$

The final value for Go is then calculated as follows:

$$Go_{final} = \frac{Gm}{(1 - a)} + Gf$$

In general, the determination of Go converges rapidly such that no more than two runs of TOPO are required in order to obtain the final temperature correction. Large differences between the value Go_{final} and the resulting corrected gradient (G_{final}) indicate disturbances due to nontopographic effects (i.e. water circulation, erosion...), or if the corrections are performed at shallow depths, that nonlinear effects are dominating (BLACKWELL & STEELE, 1980; BLACKWELL *et al.*, 1980).

For the evaluation of corrections, the time of evolution of topography was assumed to be 2 Ma. This value was deduced considering the actual erosion rates along the valleys, compared to the mountain-peaks and taking into account the maximum elevation-differences between valleys and mountains in the Alps. Although this estimation is approximate, results of a sensitivity analysis by BODMER *et al.* (1979) show little influence of a possible uncertainty of the 2 Ma value on the total correction: As long as the time of evolution of topography exceeds 1 Ma, the resulting change of the correction due to the variation of this parameter is less than 5%. The thermal diffusivity determines the penetration depth and velocity of a thermal disturbance caused by changes of relief. For an anisotropic subsurface, the component of the thermal diffusivity in the vertical direction is selected, since the calculation of BIRCH (1950) does not account for the horizontal components of the heat transfer. For this reason, the anisotropy and the orientation of the schistosity or layering has to be entered into TOPO.

4.2 Erosion correction

The topographic correction accounts only for the shape of the relief and its changes with time, but not for the removal of material. The erosional correction following CARSLAW & JAEGER (1959) and VON HERZEN & UYEDA (1963) is:

$$dT_{EROS} = Go\bar{A} + \left[(z-\bar{A}) \exp\left(-\frac{\bar{A}z}{\varkappa t}\right) \operatorname{erfc}\left(\frac{z-\bar{A}}{2\sqrt{\varkappa t}}\right) - (z+\bar{A}) \operatorname{erfc}\left(\frac{z+\bar{A}}{2\sqrt{\varkappa t}}\right) \right] (Go-Gf)/2$$

dT_{EROS}: temperature correction for uplift and erosion (sedimentation)
z: depth of measurement point
$\bar{A}$: average hight of the initial surface above reference level (z = SH, see *Fig. 9*) before the erosion
t: time since the onset of erosion
Go: initial geothermal gradient
Gf: atmospheric lapse rate
$\varkappa$: thermal diffusivity

The above equation can be used to correct for erosion, uplift and sedimentation based on the assumption that the erosion (or sedimentation) rate does not change in time. The uplift is taken into consideration by selecting appropriate values for the atmospheric lapse rate Gf: If a value for Gf is defined, the model assumes continuous erosion without uplift. If Gf is zero, a continuous uplift during the erosion is taken into account. The erosional correction is performed by the program THERM (cf. *Figure 11*). A special subroutine (SIMREG) calculates the surface temperatures and the geothermal gradient

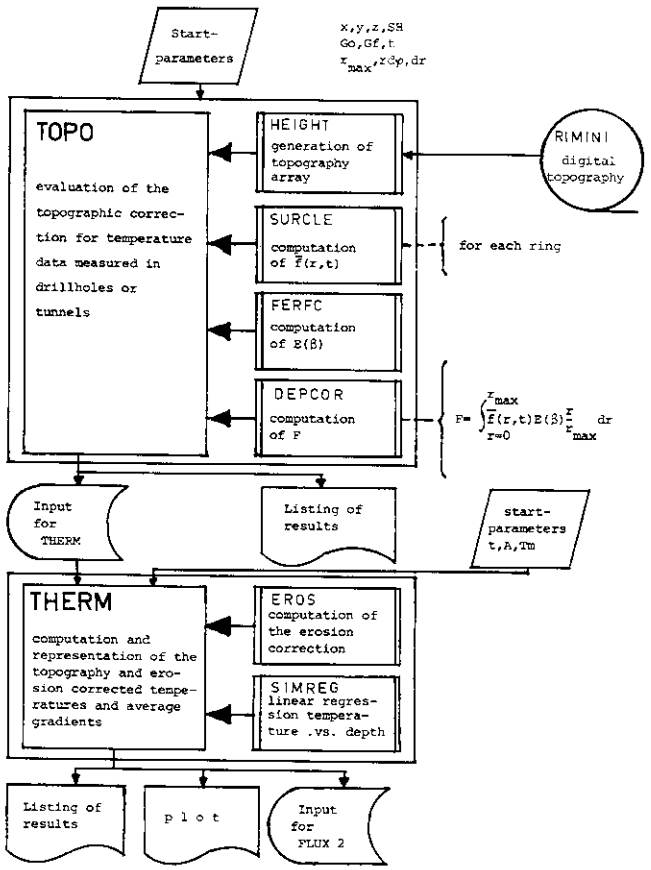

Figure 11: Flow chart for TOPO and THERM.

resulting from the uncorrected, the topographically corrected, the erosion corrected and the temperature values with all corrections applied. SIMREG does this by means of linear regression-lines through the temperature-depth-plots. In conjunction with the calculated correlation coefficients, these plots are useful for the evaluation of the quality and the effect of the corrections.

4.2.1 Evaluation of the input data

$\bar{A}$ and t strongly influence the correction (BODMER *et al.*, 1979). Since the effect of older erosional events penetrate deeper into the subsurface than very recent erosion, the erosional history for correction must be selected according to the depth of the point investigated.

A major simplification arises from the fact that the method used assumes a constant erosion rate. In reality, especially in the case of fluviatile or glacial erosion, the denudation most often acts in a differentiated manner in time and space (e.g. at the front of the glaciers): Maximum erosion rates are expected during and shortly after important uplift-episodes. In combination with increased erosion rates, however, many areas can be affected by major accumulations of detritic material.

Numerical models have been developed in order to calculate the erosional effects on subsurface temperatures in detail, and thus give more realistic temperature corrections (i.e. WERNER, 1981). In applying these models, however, a detailed knowledge of the erosional history is required. Since this history is practically never known accurately enough, the application of such models is usually not justified.

In selecting the appropriate input parameters for the erosional correction, surface observations can be used for relatively recent events. Older erosional histories can be estimated using petrographic data (i.e. FREY *et al.*, 1974; GRUENENFELDER & KOEPPEL, 1980). **Table 3** illustrates some typical values for $\bar{A}$ and t in different parts of Switzerland.

In addition to the regional erosion, local conditions have to be taken into account (RELLSTAB, 1980, unpubl.). In the vicinity of large and deep valleys which were affected by glacial erosion, local erosion rates of 300 m within the last 30 000 years are possible (BODMER *et al.*, 1979).

The impact of these "young" effects on the actual temperature field is comparable to the influence of the erosional events given in **Table 3.** Especially for tunnels, the input parameters for the erosion correction have to be evaluated with care. In addition to the regional erosion, which uniformly affects the temperature field, the isotherms near the valleys are mostly influenced by recent fluviatile or glacial erosion.

Similarly to the initial geothermal gradient in the topographic correction, Go has to be specified. This value can be calculated directly using the actual near-surface gradient:

$$Go = \left.\frac{dT}{dz}\right|_{t=0,z=0} \cdot \frac{1}{2 - 4i^2\,\mathrm{erfc}\,(p) + 4p^2}$$

with $p = \bar{A}/2\sqrt{\chi t}$.

The assumption of an initially undisturbed geothermal gradient at the beginning of an erosional event is a rather inaccurate one since many different erosional and uplift events are known to have happened during the geological history of the Alps and their Foreland. Erosional temperature corrections in the Alps have a considerable effect on the resulting temperature and on the calculated heat flow density as shown for example in comparing *Figures 17–20.* This correction is inaccu-

Table 3: Regional erosional history in different areas of Switzerland

Area	A (Elevation of initial surface above actual terrain)	t (Time elapsed since the beginning of the regional erosion)
Alps	10–20 km (RYBACH *et al.*, 1977; WERNER *et al.*, 1976)	Oligocene (30–40 mio y) TRUEMPY (1980)
Northern Foreland	Western Switzerland: 2 km Eastern Switzerland: 0.5 km (PAVONI, 1976)	Pliocene (5 mio y) HANTKE (1978)
Jura	ca. 300 m (strong local variations)	Pliocene to Miocene

rate due to the lack of precise knowledge about the erosional history.

4.3 Paleoclimatic correction

4.3.1 Introduction

Temperature fluctuations at the earth's surface can penetrate to different depths, depending on the wavelength of the fluctuations. The daily temperature variations can be measured in the uppermost few tens of centimeters only; seasonal variations penetrate, depending on rock thermal parameters, to a few tens of meters. Paleoclimatic temperature changes can be approximated by a model consisting of a series of step changes. Of course, the selection of the present mean annual temperature as reference is somewhat arbitrary; its value, however, is certainly better known than any other temperature value at any time in the past.

The temperature effect at any depth z, caused by a single step change in surface temperature, can be found by solving the one-dimensional heat conduction equation $\partial^2 T/\partial z^2 = (1/K)\partial T/\partial z$ with the step change ΔT_t, at time t' as the boundary condition:

$$\Delta T\,(z, t) = \Delta T_t, \operatorname{erf}(z/\sqrt{4\varkappa(t-t')})$$

The paleoclimatic correction dT_{palcl} for a sequence of climatic events in the past can be obtained by summation (BIRCH, 1948):

$$dT_{palcl} = Ts_1\,(1-\operatorname{erf}(z/\sqrt{4\varkappa t_1}))+$$

$$+\sum_{i=2}^{n} Ts_i\,(\operatorname{erf}(z/\sqrt{4\varkappa t_{i-1}}) - \operatorname{erf}(z/\sqrt{4\varkappa t_i}))$$

where t_i denotes the onset (before present) of the i-th climatic period with its characteristic surface temperature Ts_i.

From this data base the following four alternatives can be defined (RELLSTAB, 1981):

type O: ice-free during all glaciation periods
type R: ice-covered during the Riss period only
type RM: glaciation during Riss und Würm
type A: ice-covered during all ice ages

4.3.2 Calculation procedure

The calculation of dT_{palcl} is included in program ASSEMB (cf. *Figure 8*). For a given site the mean annual surface temperature is calculated for that locality from the data displayed in *Figure 12* by taking into account the elevation of the site and an appropriate value for the atmospheric lapse rate (generally 4.5 to 6.5 °C/km, according to location, exposition etc.). To the temperature value so calculated, 1.0 °C must be added to approximate the soil temperature (KAPPELMEYER & HAENEL, 1974, p. 93). If the standard climatic model applies to the site (i.e. for type 0), the subroutine CLIMA in program ASSEMB calculates the correction on the basis of the values given in **Table 4.**

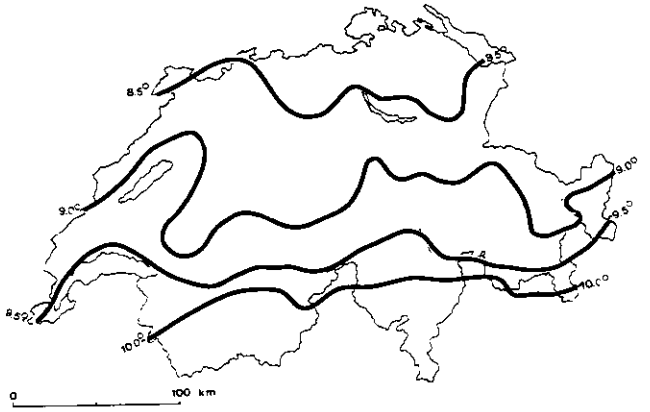

Figure 12: Mean annual surface temperature in Switzerland (after ATLAS DER SCHWEIZ 1965). Isolines indicate mean annual temperature in °C reduced to constant reference level (500 m a.s.l.).

For areas with occasional ice cover of known extent and duration, the standard model is modified according to the alternatives R, RM or A. If no data on glaciation are available, the program adjusts the climatic model by means of a special input parameter ICLIMA.

The values of thermal diffusivity and ice base temperature can be specified if local information is available. Otherwise the program calculates the paleoclimatic correction dT_{palcl} with the default values $1 \cdot 10^{-6}$ m²/s and −1 °C, respectively.

Figures 13 and 14 show some specific examples.

4.3.3 Paleoclimatic models

Instrumental records on surface temperature changes in Europe are available only for the past 200–300 years. Although there is general agreement among climatic workers that the temperature changes between the different climatic periods are relatively rapid (for

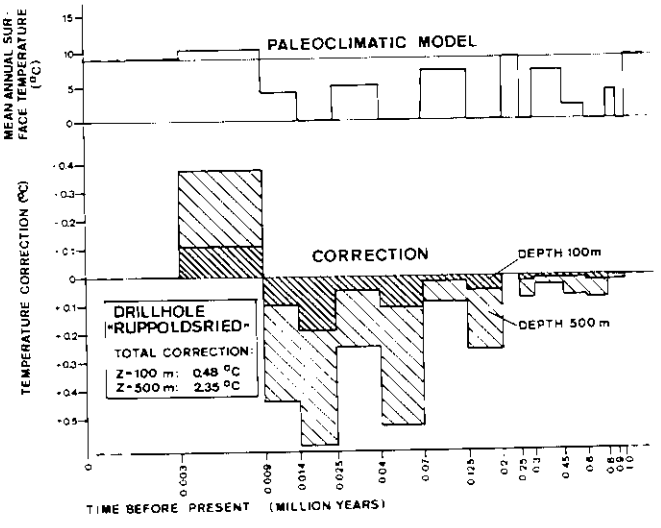

Figure 13: Paleoclimatic model and paleoclimatic temperature correction for the drillhole Ruppoldsried in western Switzerland.

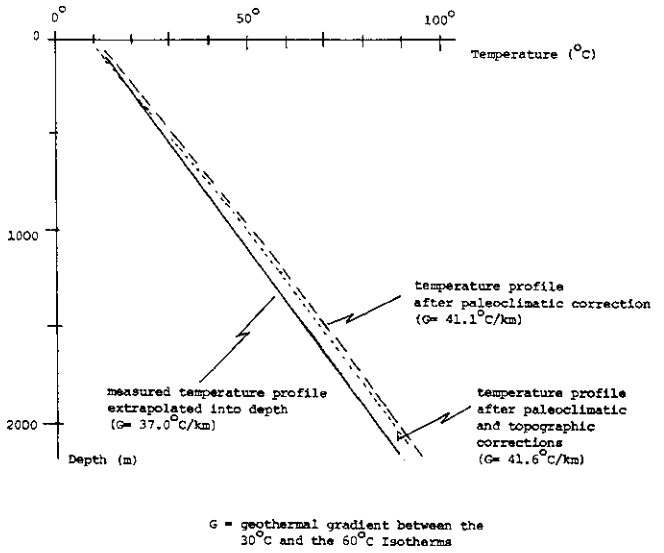

Figure 14: Topographic and paleoclimatic corrections in a drillhole.

Pleistocene transitions for the region of Zurich see PIKA, 1982), one can find different views in the literature with respect to the amplitude of paleoclimatic changes and their placing in space and time.

Nevertheless, there are numerous indicators which were used in an attempt to establish a paleoclimatic model for Switzerland (RELLSTAB, 1981, 1982) covering the following time periods:

(a) *Historical time*
- instrumental records
- chronicles, harvest reports, glacier movements

(b) *Holocene and Quarternary*
- dendrochronology
- ice and snow stratigraphy in polar ice
- biostratigraphy (pollen; micro- and macrofossils)
- O^{18}/O^{16} isotope ratio (in dated sediments, ice and fossils)
- sedimentology
- geomorphology

The extensive literature surveyed to establish a paleoclimatic model includes LAMB (1977), FRAKES (1979), HANTKE (1978), SCHWARZBACH (1961), and OESCHGER *et al.* (1980). The model has been compared to other paleoclimatic models in Europe (VASSEUR, France; GRUBBE, FRG; BALLING, Denmark; data from ČERMÁK, 1982: Circular for Standardization).

The paleoclimatic model used to calculate the correction dT_{palcl} is given in **Table 4** and in *Figure 13* (top).

The temperatures during the different climatic periods of the model relate to today's local mean annual surface temperature and show clearly the importance of glacial periods ("ice ages") which led to severe glaciations in large areas in Switzerland.

Parametric studies (RELLSTAB, 1981) led to an optimum number of 29 climatic periods. In general,

Table 4: Paleoclimatic model for Switzerland (RELLSTAB, 1981, 1982)

Step	Time range	(Years before present)	Relative temperature	Period of glaciation
1	0 –	50	0.0	
2	50 –	80	– 0.4	
3	80 –	170	– 0.8	
4	170 –	200	– 0.6	
5	200 –	230	– 0.7	
6	230 –	280	– 0.8	
7	280 –	400	– 0.1	
8	400 –	650	– 0.7	
9	650 –	850	+ 0.4	
10	850 –	1 000	– 0.3	
11	1 100 –	2 000	0.0	
12	2 000 –	3 200	– 0.5	
13	3 200 –	5 000	+ 0.5	
14	5 000 –	8 000	+ 1.5	
15	8 000 –	10 000	0.0	
16	10 000 –	14 000	– 6.0	
17	14 000 –	25 000	– 13.0	Würm
18	25 000 –	40 000	– 4.0	
19	40 000 –	70 000	– 11.0	Würm
20	70 000 –	125 000	– 2.0	
21	125 000 –	200 000	– 13.0	Riss
22	200 000 –	250 000	– 2.00	
23	250 000 –	300 000	– 13.0	Mindel
24	300 000 –	450 000	– 2.0	
25	450 000 –	600 000	– 7.0	
26	600 000 –	800 000	– 10.0	Günz
27	800 000 –	900 000	– 5.0	
28	900 000 –	1 000 000	– 10.0	Günz
29	1 000 000 –	∞	0.0	

recent changes are known more accurately than earlier events. However, these studies revealed that climatic changes during the time period 0–10 000 a b.p. are significant only for correcting temperature measurements in shallow boreholes, the most important period being the time 10 000–100 000 a b.p., which therefore must be subdivided in a more sensitive way than the times before and after this period. Climatic changes older than 1 m.a. can be neglected for the model applied.

4.3.4 The influence of ice cover

It is now widely accepted that in glaciated areas the ice cover supplied considerable thermal insulation against the (at times) low ice-age temperatures. For the present calculations a constant rock surface-temperature of –1 °C was assumed.

In calculating paleoclimatic corrections for a given drillhole site this must be taken into account by specifying the time intervals when "protecting" ice cover existed in that area and when it was ice-free. HANTKE (in TRUEMPY, 1980) designed a map showing the maximum areal extent of glaciation in Switzerland during the main ice ages. There is evidence that the extent of ice cover was roughly the same during the Riss and the Mindel periods and during the Günz and Würm periods.

5. Heat flow density determination

5.1 Introduction

The heat production within the earth is largely due to radioactive decay of unstable isotopes, mainly U, Th and K. The elevated temperatures within the earth compared to the relatively low atmospheric temperatures give rise to a steady terrestrial heat flow which has a worldwide average value of 75 mW/m² at the earth's surface. The temperature increase with depth (geothermal gradient) on the continents is approximately 30 °C/km in the upper few kilometers of the earth's crust. The radioactive isotopes are mainly concentrated in the upper continental crust. Due to this, both the geothermal gradient and the terrestrial heat flow decrease continuously with depth.

The most significant heat transfer mechanisms in the subsurface are conduction and natural or forced convection. The convection within the upper crust is very often related to water circulation through rock pores or along fractures. In general, the hydrogeological conditions of the subsurface are not known well enough to calculate the convective heat transfer. Therefore it is most often estimated by modelling. The conductive heat transfer is determined by the thermal conductivity distribution within the subsurface (see chapter 3.2).

The conductive heat flow density q (HFD), defined as the heat flow per unit area (W/m²), is determined as follows:

$$q = K\nabla T \doteq K\frac{dT}{dz}$$

K : rock thermal conductivity (W/m°K)

$\frac{dT}{dz}$: geothermal gradient (°C/m)

This "FOURIER" formula can be derived from the heat transport equation under simplified conditions (e.g. one dimensional flow, stationary conditions etc.). The assumption of pure conduction is usually justified if the surface HFD is constant with depth and if no major lateral thermal conductivity variations occur.

Since in many cases the convective heat transfer is much more effective than the conductive one, the detection of water circulation systems is possible, because they create strong local (horizontal and/or vertical) variation of the temperature field and of the HFD, especially in and near discharge and recharge areas.

The terrestrial heat flow density cannot be measured directly at a specific point. It has rather to be determined using a temperature profile over a relatively large distance, being preferably oriented parallel to the heat flow. The temperature gradient in conjunction with the rock thermal conductivity along the profile will provide a value for the average HFD across the section investigated. For the correction of inclined temperature profiles, the direction of the terrestrial heat flow is usually assumed to be vertical.

If important radioactive heat production changes occur within the measured profile, these effects have to be taken into consideration as well. As demonstrated in BODMER (1982), these heat sources can be neglected at most heat flow sites in Switzerland.

The numerical processing of the above mentioned formula for calculating the HFD can be performed in different ways (see RYBACH & BODMER, 1983). The choice of the most suitable technique is dependent on the temperature and thermal conductivity data, the sampling rate and the data quality.

For the HFD determinations in Switzerland, the "BULLARD PLOT" technique was selected as the most reliable and useful one (BULLARD, 1939). Each temperature value is plotted versus the thermal resistance between the earth's surface and the depth of the temperature measurement. The slope of the regression line is proportional to the HFD. This method provides good results, especially in deep holes where the data quality usually decreases with depth. Furthermore, this calculation method can be applied to all data categories.

Experience in interpreting heat flow data in specific areas has shown that in many cases the changes in temperature gradient with depth are not only due to changes in thermal conductivity, but are the result of various effects like measurement errors, incomplete corrections, water circulation, thermal disequilibrium during the measurements etc. A statistical approach to evaluate the heat flow density, therefore, is considered to be much more realistic than conventional processing techniques. Furthermore, much useful information about the data quality can be derived from the regression technique, e.g. the correlation coefficient for the evaluation of the input data quality, the statistical error of the slope of the regression line, giving a measure of the quality of the heat flow density determination, or the results of regressions of higher order to analyse the curvature of the Bullard Plot in order to obtain information e.g. about possible water circulation.

5.2 Data processing

5.2.1 Heat flow density computations

The HFD calculations are performed by the program FLUX2 (*Figure 15*). This program is loaded automatically after the temperature corrections are calculated (see chapter 3 and *Figure 8*).

FLUX2 reads the corrected temperature delivered by program THERM2. Using the borehole data (subroutine GEOL and subroutine LEIT), a conductivity profile of the site investigated is constructed. In most cases no core material was available for thermal conductivity measurements. The conductivity profile, therefore, was estimated from the stratigraphic/lithologic profile of the hole and a thermal conductivity catalogue of Swiss rocks. Using this profile, the thermal resistance for the depth of each temperature measurement are calculated and the Bullard Plot is constructed (subroutine BULL). The HFD and the statistical error is calculated by the subroutine SIMREG. The final results are listed and a plot is drawn (see *Figure 16*).

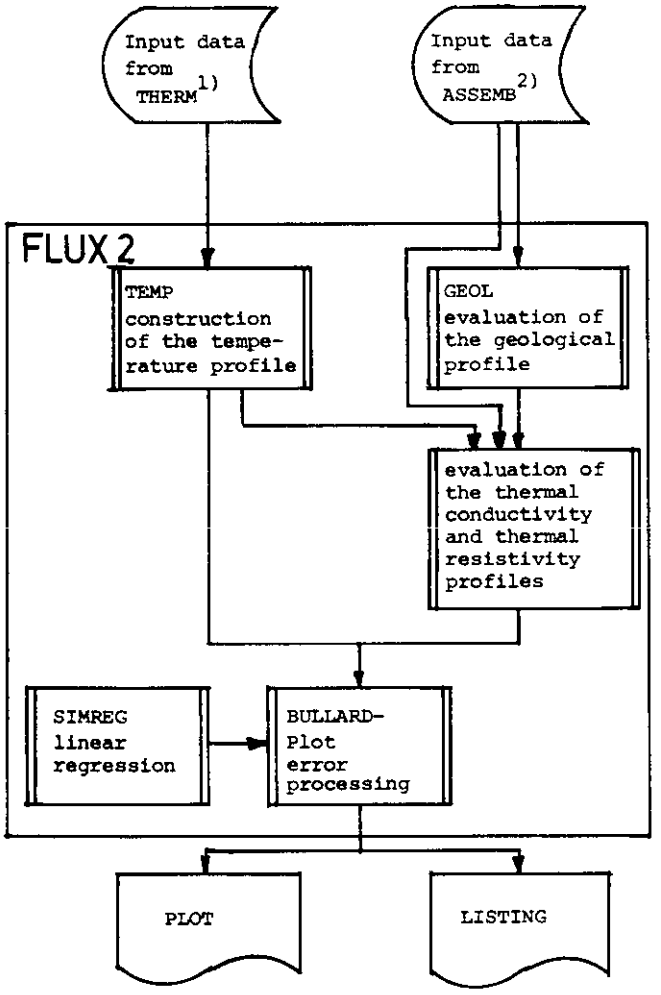

Figure 15. Flow chart for the heat flow density calculation.

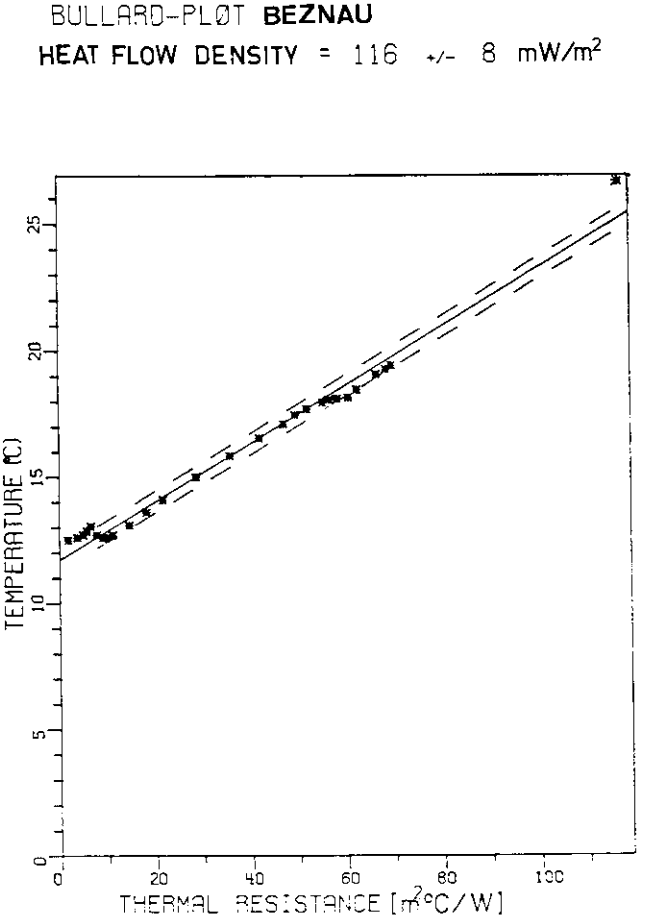

Figure 16. Bullard plot for drillhole Beznau.

5.2.2 Contouring of the isolines

The HFD determinations in Switzerland are unevenly distributed. Manual interpolations to determine the course of isolines would introduce bias of unknown extent since the interpreter is usually influenced by physiographic units, geologic boundaries etc. Therefore, automatic contouring by computer was applied on the basis of a contour interval of 10 mW/m² which corresponds to the general accuracy of the individual heat flow determinations.

Computer contouring is now standard practice in many kinds of geophysical mapping. Computer codes developed for the Gravity Maps of Switzerland (KLINGELE & OLIVIER, 1980) were adapted to heat flow density mapping. The construction of isolines is based on interpolation, within a circle with a radius of R_o, of the measured HFD values to points of a quadratic grid (spacing d), according to the method of LAPORTE (1962). A smoothing factor η was introduced, as was a threshold of elimination, β. For this procedure, all heat flow density data were equally weighted.

The data density is about one HFD value per 400 km² in the mapped area (regions with isolines on the Geothermal Map of Switzerland). Parametric studies revealed the following optimum values: $R_o = 70$ km, d = 10 km, $\eta = 0.1$ and $\beta = 10\%$. The HFD values in the neighbouring regions of France and Germany are mainly from GABLE (1979), VASSEUR (1982) and HAENEL (1980).

5.3 Results

The HFD determinations were only carried out on data from drillholes, tunnels and shafts if the temperature measurements were reliable and if no major convective disturbances were detected. The HFD maps of *Figures 17 to 20* were constructed on the basis of about 100 observations on sites located in Switzerland and about 50 in neighbouring areas.

The input data base was further enlarged for the construction of the HFD map 1 : 500 000 by the results of numerous lake bottom measurements (FINCKH, 1981) and by the data from GABLE (1979), VASSEUR (1982) and HAENEL (1980).

In most cases the lake measurements show higher HFD values than the surrounding drillholes. In order to clarify these discrepancies, a 200 m deep drillhole was placed next to a lake measurement site in the lake of Zurich (drillhole "ZUBO 80", FINCKH & HSU 1984). The HFD determined in that hole (125 mW/m²) is in agreement with the results of the measurements in lake bottom sediments (118–125 mW/m²), proving that the two techniques provide comparable HFD values.

The difference of HFD between lakes and their surroundings can be interpreted as a result of water migration due to the deep V-shaped bedrock cross section and, in many cases, due to the location of the lakes along fracture zones.

Four different values of the HFD were calculated, including i) uncorrected temperatures, ii) temperatures corrected for the effect of topography, iii) temperatures corrected for topography and paleoclimate, and finally iv) temperatures corrected for topography, paleoclimate and erosion.

The four data categories are documented in isoline maps which demonstrate the influence of different corrections on the isoline pattern (*Figures 17–20*). The data base used for the construction of these preliminary maps differs slightly from map to map and significantly from the final HFD representation on the 1 : 500 000 scale. The data base is as follows: *Figure 17:* 75 drillholes; *Figure 18:* 77 drillholes, 4 tunnels ; *Figure 19:* 79 drillholes, 36 lake determinations; *Figure 20:* 53 drillholes; map 1 : 500 000: 109 drillholes, 38 lake determinations, 8 tunnels.

The comparison of these maps shows that they are predominantly affected by topography effects along the Alps. For the final representation of the HFD on a 1 : 500 000 scale (Geothermal Map of Switzerland), only the topographic correction was carried out according to common practice. By this means the Swiss HFD map is comparable to other European HFD maps.

The uncertainty of each HFD value was estimated from the scatter around the regression line which defines the heat flow density (see chapter 5.1). This statistical approach was chosen, because the uncertainty in HFD is dependent on unpredictable effects, such as water convection, local variations of thermal conductivity etc.

Figure 21 shows the error distribution of the heat flow density determinations. Considering that the estimated error of most determinations is less than 10 mW/m², the isoline spacing chosen was 10 mW/m². Furthermore, the figure shows that the data quality strongly depends on the temperature data category (see chapter 3.1) used. The continuous temperature measurements usually provide more reliable heat flow density data with uncertainty less than 10 mW/m², whereas the other data (BHT-values, single values, tunnel data) often are more uncertain. In some cases, the data quality was too poor for the accurate construction of a regression line (significance level 5%). These data are shown on the right hand side of the histogram.

The errors of the data taken from the literature (VASSEUR, 1982; FINCKH, 1981; HAENEL, 1980 and GABLE, 1979) were not analysed and thus are not shown in *Figure 21.*

5.4 The Geothermal Map of Switzerland

The Geothermal Map of Switzerland 1 : 500 000 has been constructed on the basis of the complete data set given in *Appendix 3.* In order to make the map compatible with other European HFD maps, only the topographic correction has been applied to the data. The isolines of the Swiss HFD map cover the major part of the country. The remaining areas are located in the Eastern Alps (Grison) and in the southwestern edge of the country (Valais). As illustrated in *Figure 21*, most heat flow sites reach depths less than 500 m. Only a few boreholes – mostly hydrocarbon exploration boreholes – are deeper (maximum: 5.5 km).

The average HFD, corrected for the irregular distribution of the observation sites, is 83 mW/m² and shows a general decreasing trend from the Northern Foreland (av. value 88 mW/m²) to the Alps in the south (av. value 77 mW/m²). This trend is overlain by a couple of distinct positive and negative anomalies, especially along the Jura chain and the Alpine border. These anomalies are thought to result from forced water convection, because many of them coincide with the occurrence of thermal or subthermal water and with abnormal chemical compositions of many surface waters (isotopic evidence, geochemical reservoir temperatures). The two most pronounced anomalies are located in the area Baden – Zurzach – Schinznach, near the northern border of Switzerland, and in the area of St. Gallen in the east. Both anomalies have been analysed carefully (see NEFF, 1981; ANGEHRN & BODMER, 1982, 1984) and the interpretation of the HFD pattern is discussed in BODMER & RYBACH (1985).

Water seepage velocities (= Darcy velocities) of a few mm/year can already give rise to such anomalies. Zones in which a strong local variation of the geothermal conditions are expected due to water circulation are

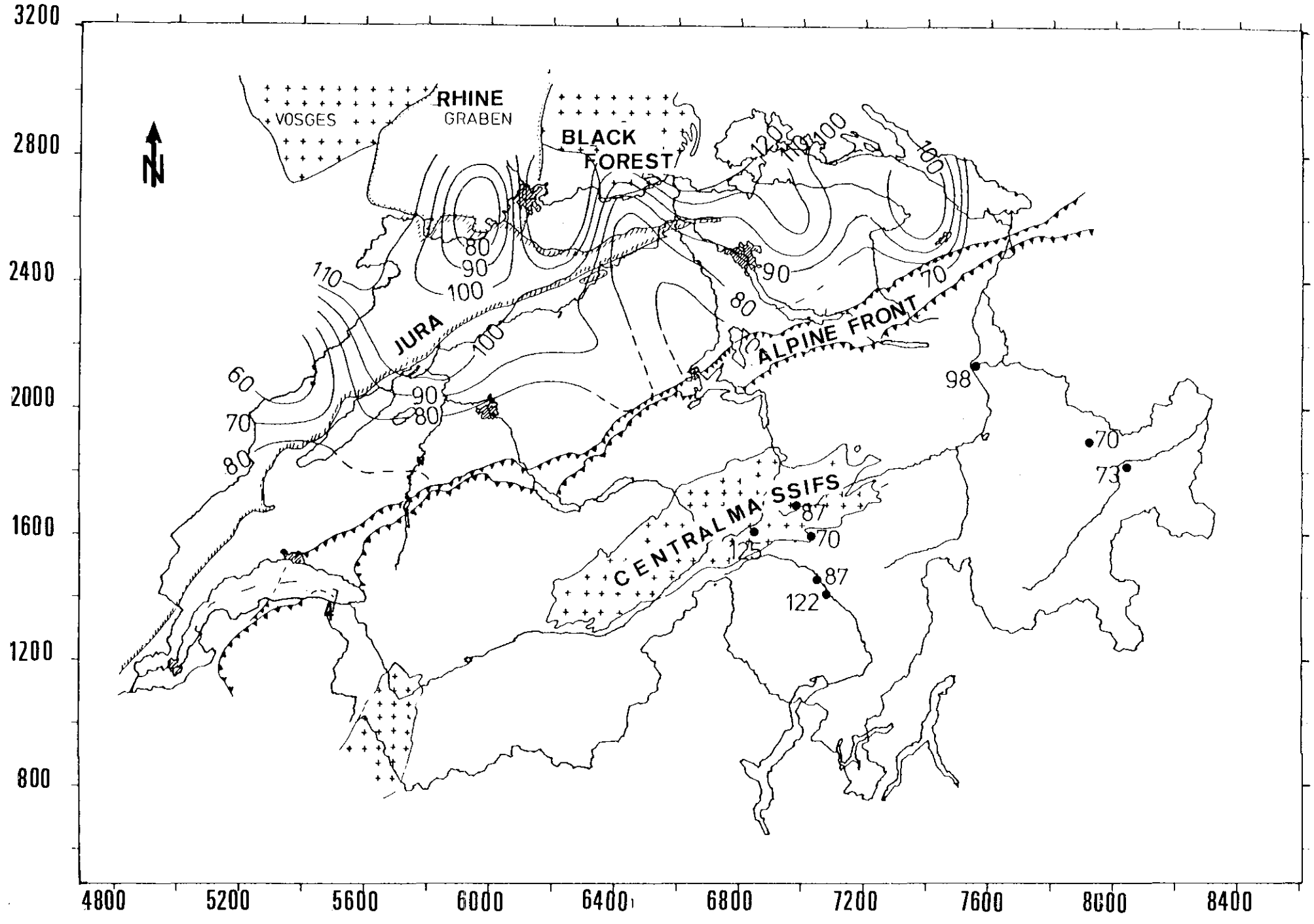

Figure 17: HFD map of Switzerland, uncorrected data (mW/m²).

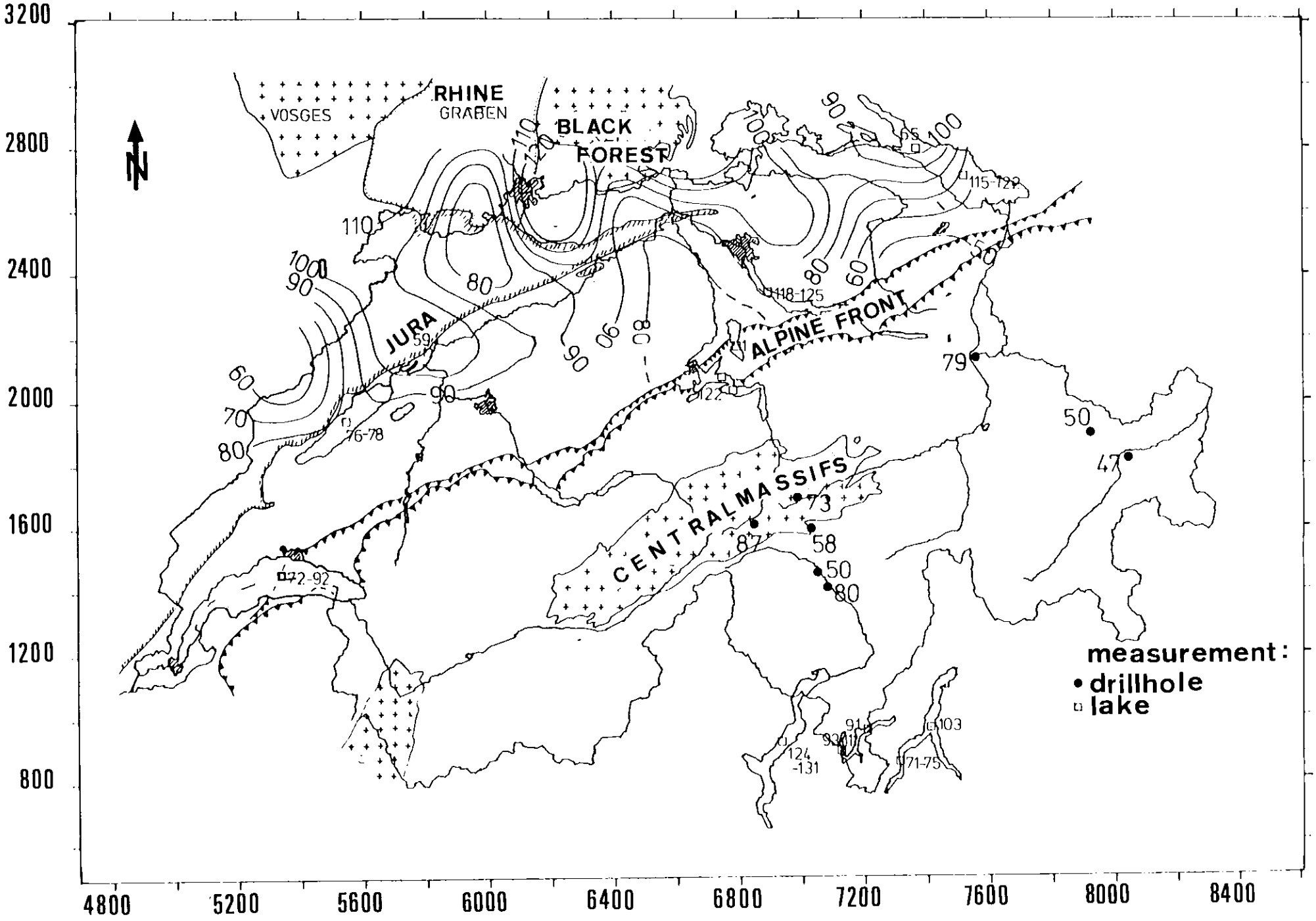

Figure 18: HFD map of Switzerland, data corrected for topography (mW/m²).

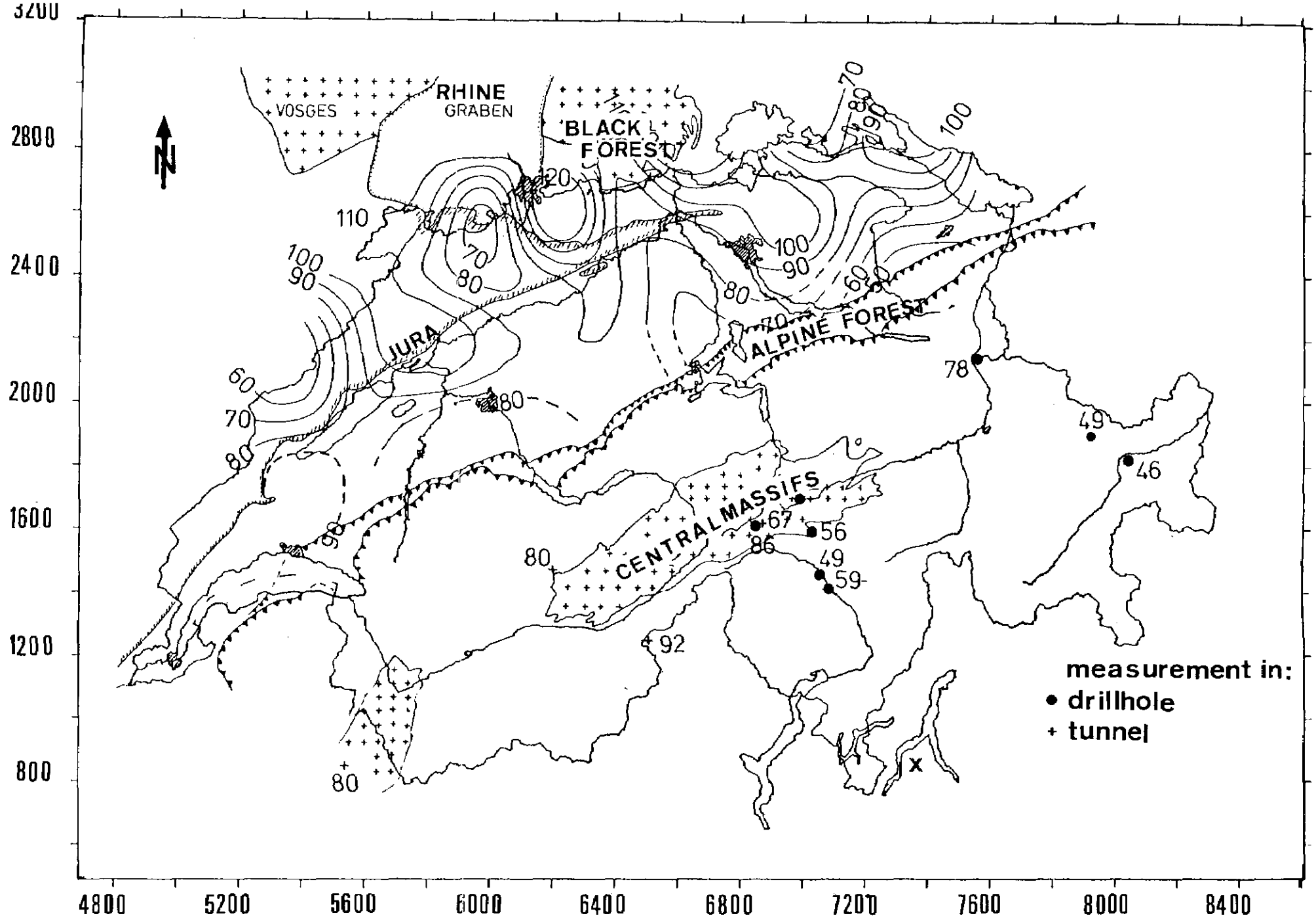

Figure 19: HFD map of Switzerland, data corrected for topography and paleoclimate (mW/m²).

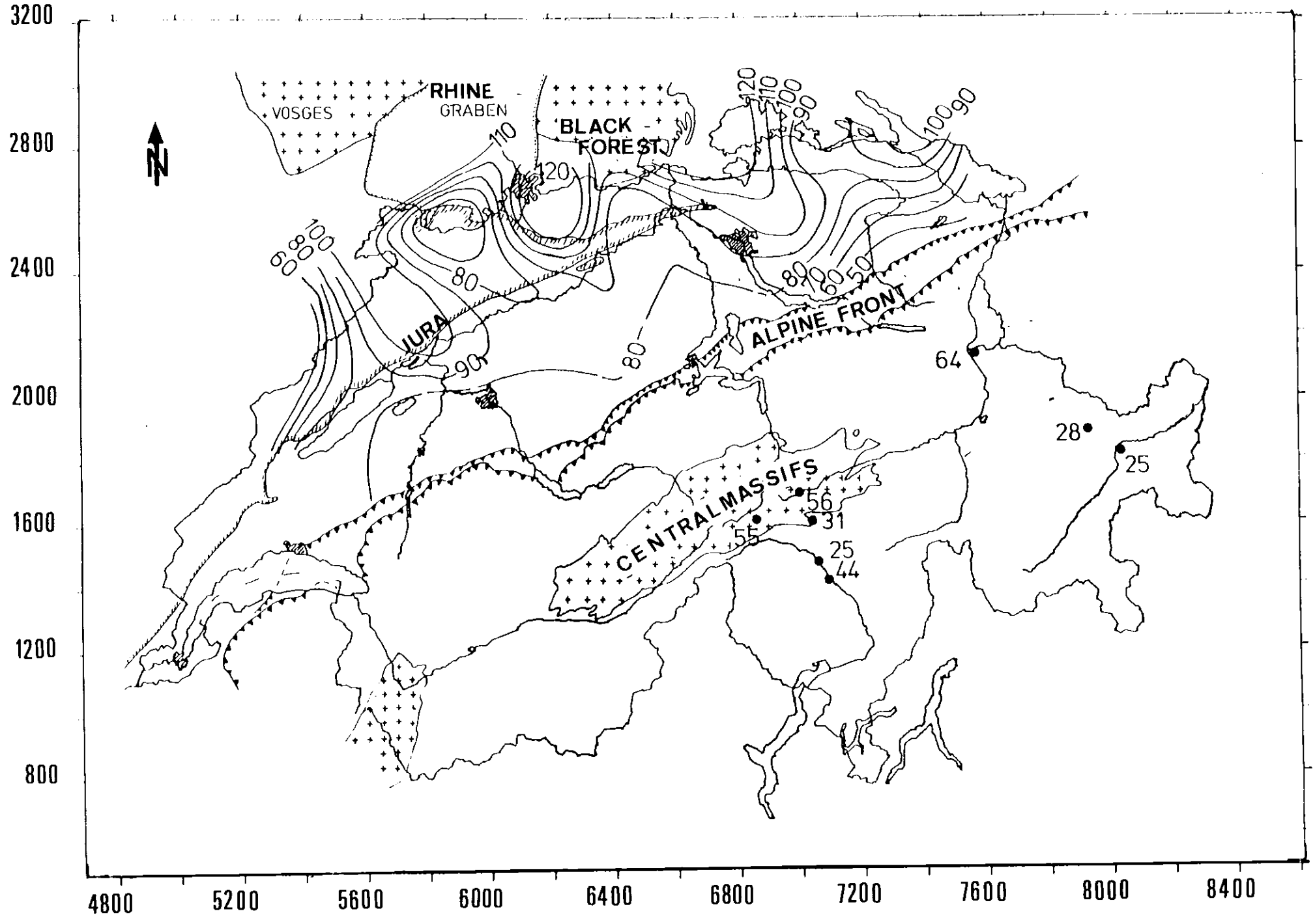

Figure 20: HFD map of Switzerland, all corrections applied (mW/m²).

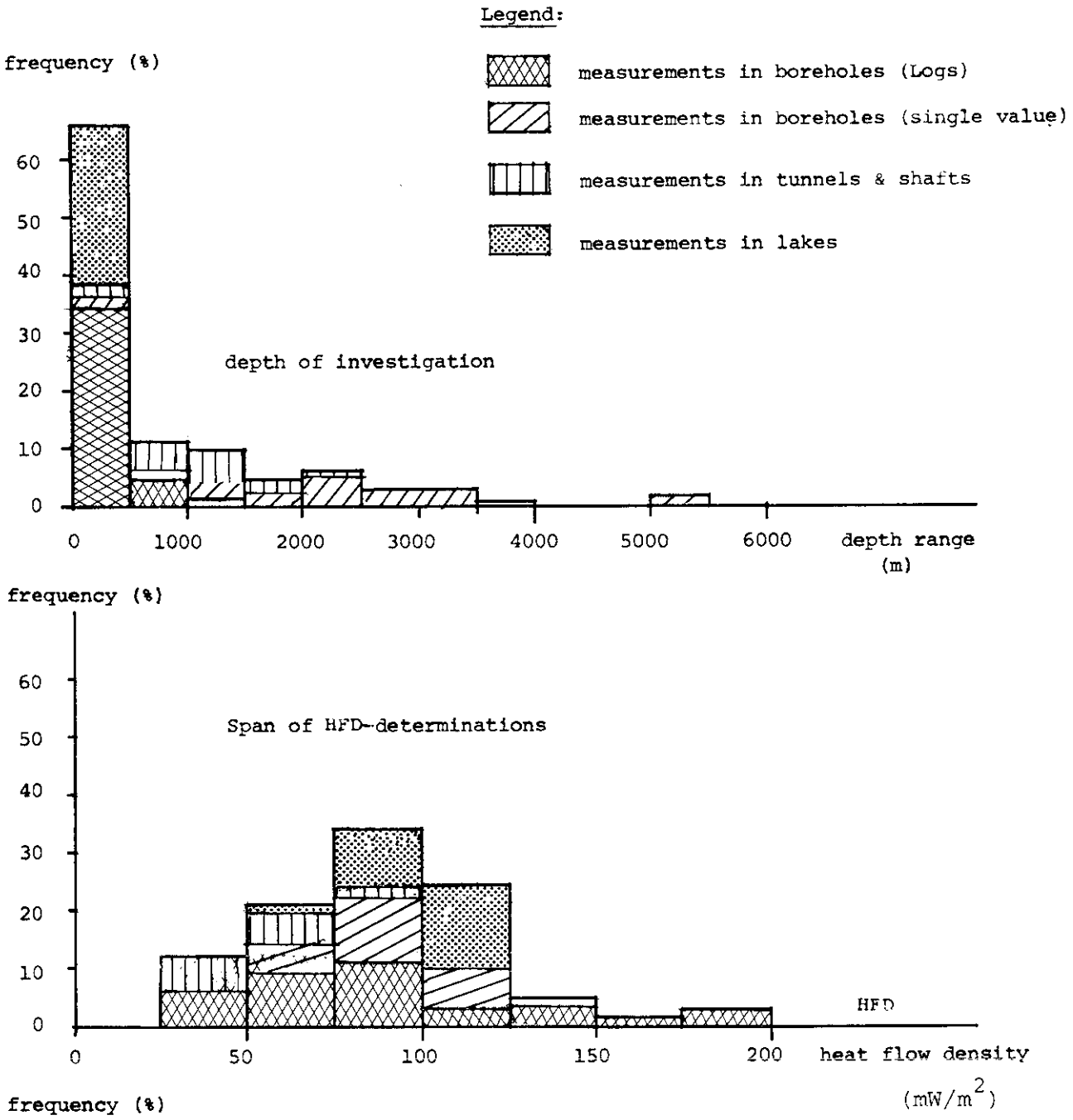

Figure 21: Statistics of Swiss HFD data.

especially delineated on the HFD map. These areas are mainly located along the southeastern edge of the Folded Jura and along the Rhine and Rhône valleys in the Alps. In addition, several other circulation systems on a more local scale may exist, but could not been identified on the basis of the available geothermal information.

5.5 Comparison with the results of other countries

HFD maps have been published for most countries in Europe. In order to enable a comparison of the different results or to construct general maps on the continental scale (ČERMÁK, 1979; HAENEL, 1980), it is essential that processing techniques are similar. It is, therefore, important to verify how well the results presented fit with the data from other countries or the international guidelines (see BALLING *et al.*, 1981).

Tables 5 and 6 demonstrate the differences in the methodology of processing and the data density of the HFD maps in different European countries.

In most cases, different categories of temperature data were used and the results were combined. However, the corrections applied to these data do not generally agree. The most significant discrepancy lies in the application and calculation of the topography correction. It must be noted, however, that in many countries with low relief, the topographic and the erosional corrections are small and often negligible.

Major differences between the authors lie in the determination of the thermal conductivity. Many different measuring techniques have been used and many HFD values have been obtained, using estimates for the thermal conductivity. Since the measuring technique has to be adapted to the nature of the heat flow site (lake, borehole, tunnel), and since suitable rock samples are not always available (i.e. core material from drillholes), general standardisations are not useful.

Table 6 compares the data density used for the construction of the European geothermal maps (see ČERMÁK, 1979). Except for the German Democratic Republic, the data density of Switzerland is much higher than in the other countries.

Table 5: Comparison of the methodology of HFD determination in different European countries

Country	Temperature			Thermal conductivity			Correction				References
	D	T	L	NP	TR	DB	TO	PC	ER	D	
Belgium	+	–	–	–	–	–	–	–	–	–	GRAULICH 1969 LEGRAND 1985
F. R. of Germany	+	+	+	+	+	+	+	–	–	+	BRAM 1979
Denmark	+	–	–	+	+	+	–	+	–	+	BALLING 1979
German D.R.	+			not specified							HURTIG & OELSNER 1979
France	+	–	+	–	+	+	+	+	–	–	VASSEUR 1981
Great Britain	+	+	–	–	–	+	+	+	–	–	BLOOMER *et al.* 1979
Italy	+	–	+	+	–	+	not systematic				LODDO & MONGELLI 1979
Holland	+	–	–	–	–	–	–	–	–	–	THIADENS 1968 SADEE 1975 v. ENGEN 1975 DALFSEN 1981
Austria	+	–	+	+	–	–	not systematic				HAENEL & ZOTH 1973 BOLDIZSÁR 1968
Switzerland	+	–	–	–	+	–	+	+	+	–	BODMER 1982
	–	+	–	–	+	–	+	+	–	–	RYBACH & FINCKH 1979
	–	–	+	+	–	–	+	+	–	+	FINCKH 1981
Spain	+	–	–	–	–	–	–	–	–	+	ALBERT-B. 1979
Czechoslovakia	+	–	–	–	+	+	+	+	–	–	ČERMÁK 1979
Hungary	+	+	–	–	+	+	–	–	–	+	HORVÁTH *et al.* 1979

Legend:
Temperature measurements: D = drillholes T = tunnels and shafts L = lakes
Thermal conductivity: NP = needle probe TR = transient method DB = "divided bar" method
Corrections applied: TO = topography PC = paleoclimate ER = erosion D = misc. (e.g. sedimentation)

Table 6: Data density and average HFD in different European countries

Country	surface (km^2)	Q* mW/m^2	number of values	data density per 10^4 km^2
Belgium	30507	ca. 55	–	–
F. R. of Germany	248454	67	175	1.6
Denmark	43042	61	36	8.4
German D. R.	108273	83	348	32.1
France	551603	99	133	2.4
Great Britain	244016	68	71	2.9
Italy	301218	69	62	2.1
Holland	36127	55	6	1.7
Austria	83849	72	51	6.1
Switzerland (total)	41488	83	104	25.1
Alps**)	23530	77	31(24)	13.2 (10.2)
Foreland	17758	88	73	41.1
Spain	504741	82	133	2.6
Czechoslovakia	127859	74	112	8.8
Hungary	93030	95	27	2.9
USSR (Europ. part)	5570000	52	761	0.1

*Values taken from ČERMÁK (1979) (except for Switzerland)
**Value for Alps + lake measurements in Southern Switzerland.
Values in brackets: Alps only

6. Conclusions

The average heat flow density in Switzerland amounts to about 85 mW/m^2, within a width of variation from 40 mW/m^2 to 160 mW/m^2. The estimated error of the contoured isolines apart from areas with strong water circulation effects (which are shown on the map) is expected to be less than $\pm$ 10 mW/m^2.

The surface heat flow density pattern in Switzerland clearly displays a general trend: the heat flow density values decrease from north to south towards the Alps, reach a minimum there and increase again further south. Superimposed on this regional trend are several local anomalies, positive and negative, which can be attributed to thermal effects of deep groundwater circulation. Groundwater seepage velocities in the order of only a few mm/year can already cause anomalies of the observed strength.

The heat flow density map displays the actual state of knowledge of the regional geothermal conditions in Switzerland. Since the data base used is small compared to other geophysical maps, and since the quality of some data is poor, the introduction of new data may have considerable effects on the course of the isolines. This is especially the case in the Alps and the Jura with generally rather low data density and where major local disturbances of the geothermal conditions of the subsurface can be expected. It is, therefore, indispensable that the Geothermal Map of Switzerland is revised periodically on the basis of new data collected by or communicated to the authors of the present map. The data processing technique developed allows for rapid and efficient updating.

References

ALBERT-BELTRAN J. F. (1979): Heat Flow and Temperature Gradient Data from Spain. In: Čermák, V. & Rybach, L. (eds.): Terrestrial Heat Flow in Europe. Springer, Heidelberg, 261–266.

ANGEHRN P., BODMER Ph. (1982): Generelles Prospektionsprogramm Geothermik für das Gebiet des Kantons St. Gallen. Untersuchungsabschnitt Fürstenland. Baudepartement des Kantons St. Gallen (Report), 100 p., 69 ann. (2 vols).

ANGEHRN P., BODMER Ph. (1984): Generelles Prospektionsprogramm Geothermik für das Gebiet des Kantons St. Gallen. Untersuchungsabschnitte Rheintal, Seetal, Gaster, See & Toggenburg, Baudepartement des Kantons St. Gallen (Report) 88 p., 125 ann. (2 vols).

ATLAS DER SCHWEIZ 11: Klima und Wetter I (1965). Bearbeiter: Max Schuepp, Theodor Zingg.

BALLING N. (1979): Subsurface temperatures and heat flow estimates in Denmark. In: Čermák, V. & Rybach, L. (eds): Terrestrial Heat Flow in Europe. Springer, Heidelberg, 161–171.

BALLING N., HAENEL R., UNGEMACH P., VASSEUR G., WHEILDON J. (1981): Preliminary guidelines for heat flow density determination. Commission of the European Communities, EUR 7360 EN, 32.

BIRCH F. (1948): The effect of Pleistocene climatic variations upon geothermal gradient, Am. J. Sci., 246, 729–760.

BIRCH, F. (1950): Flow of Heat in the Front Range, Colorado. Bull. Geol. Soc. Am. 61, 567–630.

BLACKWELL D. D., STEELE J. L., BROTT C. A., (1980): The terrain effect on terrestrial heat flow. J. Geophys. Res, 85, 4757–4772.

BLOOMER J. R., RICHARDSON S. W., OXBURGH E. R. (1979): Heat flow in Britain: an assessment of the values and their reliability. In: Čermák, V., Rybach, L. (eds.): Terrestrial Heat Flow in Europe, Springer, Heidelberg, 293–300.

BODMER Ph., OTTINGER Th., RYBACH L. (1976): Sammlung geothermischer Daten in der Schweiz, Zwischenbericht an das BEW, 21 p.

BODMER Ph., ENGLAND P. C., KISSLING E., RYBACH L. (1979): On the correction of subsurface temperature measurements for the effects of topographic relief. Part II: Application to temperature measurements in the Central Alps. In: Čermák, V., Rybach, L. (eds.): Terrestrial Heat Flow in Europe, Springer, Heidelberg, 78–87.

BODMER Ph. (1980): Die Bohrung Nr. 7904 der NOK: Wärmeleitfähigkeitsmessungen an den Bohrkernen. Interner Bericht NEFF 030, 9 p.

BODMER Ph., SCHÄRLI U. (1980): Wärmeleitfähigkeitskatalog. Interner Bericht NEFF 024, 15 p.

BODMER Ph. (1982): Beiträge zur Geothermie der Schweiz. Ph. D. thesis no. 7034, ETH Zurich.

BODMER, Ph., RYBACH, L. (1983): Processing and representation of heat flow density maps – Part I: Subsurface temperatures and thermal conductivities. Zbl. Geol. Paläont. Teil I, 80–86.

BODMER Ph., RYBACH L. (1985): Heat flow maps and deep groundwater circulation. J. Geodyn. (In press).

BOLDIZSÁR T. (1968): Geothermal data from the Vienna basin. J. Geophys. Res. 73, 613–618.

BRAM K. (1979): Heat Flow Measurements in the Federal Republic of Germany. In: Čermák, V. & Rybach, L. (eds.): Terrestrial Heat Flow in Europe. Springer, Heidelberg, 191–196.

BÜCHI U. P., BODMER, Ph. (1983): Der Tiefenverlauf der seismischen Geschwindigkeiten in den Molassesedimenten des schweizerischen Mittellandes. Bull. Ver. Schweiz. Petrol.-Geol. u. -Ing. 49, 3–14.

BULLARD E. C. (1939): Heat flow in South Africa. Proc. Roy. Soc. London, Ser. A., 173, 474–502.

CARSLAW, H. S., JAEGER, J. C. (1959): Conduction of heat in solids. Oxford. University Press, 386 p.

ČERMÁK V. (1979): Heat flow map of Europe. In: Čermák, V. & Rybach, L. (eds.): Terrestrial Heat Flow in Europe, Springer, Heidelberg, 1–49.

ČERMÁK V., RYBACH L., eds., (1979): Terrestrial Heat Flow in Europe. Springer, Heidelberg, 326 p.

CLARK S. P., NIBLETT E. R. (1956): Terrestrial heat flow in the Alps. R. Astr. Soc. Mon. Not. 7, 176–195.

CLARK S. P., JAEGER E. (1969): Denudation rate in the Alps from geochronologic and heat flow data. Am. J. Sci. 267, 1143–1160.

DALFSEN v. W. (1981): Geothermal investigation in shallow observation wells. Rep. Groundwater survey TNO. Proj. G/A 9. 95 p.

ENGEN v. H. (1975): An interpretation of Groningen subsurface temperature data. Geol. Mijnbouwh 54, 177–183.

DE LA RUE A., MARCET F. (1834): Quelques observations de physique terrestre. Mém. Soc. Phys. Genève.

ENGLAND P. C. (1976): Ph. D. Thesis. Oxford univ. Thermal modelling from heat flow and velocity modelling from seismological data with special reference to the Eastern Alps. 253 p.

FINCKH P. (1981): Heat flow measurements in 7 perialpines lakes in Switzerland: Summary. Geol. Soc. Am Bull. 92, 108–111.

FINCKH P., HSÜ K. J. (1984): Heatflow of the Lake Zurich region, a comparison of lake-based and land-based measurements. In: Hsü K. J., Kelts K. R. (eds.): Quaternary Geology of Lake Zurich: An Interdisciplinary Investigation by Deep-Lake Drilling. Schweizerbart, Stuttgart, 157–160.

FRAKES L. A. (1979): Climates throughout Geologic Time. Elsevier, 1979 amsterdam, 310 p.

FREY M., HUNZIKER J. C., FRANK W., BOCQUET J., DAL PIAZ G. V., JAEGER E., NIGGLI E. (1974): Alpine Metamorphism of the Alps: A review. Schweiz. Min. Per. Mitt. 54, 254–269.

GABLE R. (1979): Draft of a geothermal flux map of France. In: Čermák, V., Rybach, L. (eds.): Terrestrial Heat Flow in Europe, Springer, Heidelberg, 179–185.

GRAULICH J. M. (1969): Eaux minérales et thermales en Belgique. XXIII Int. Geol. Congr. 18. 9–15.

GRUBBE K., HAENEL, R., ZOTH, G. (1983): Determination of the vertical component of thermal conductivity by line source methods. Zbl. Geol. Paläont. I. 49–56.

GRÜNENFELDER M., KÖPPEL V. (1980): Geochronological data. In: Trümpy (1980), 87–89.

HAENEL R., ZOTH G. (1973): Heat Flow Measurements in Austria and Heat Flow Maps of Central Europe. Z. Geophys. 39, 425–439.

HAENEL R. (1980): Atlas of subsurface temperature in the European Community, Commission of the European Communit, Directorate-General for Research, Science and Education, Luxemburg. 43 p.

HANTKE R. (1978): Eiszeitalter: Die jüngste Erdgeschichte der Schweiz und ihrer Nachbargebiete. Ott, Zürich, Bd. I, 468 p.

HASHIN Z., SHTRIKMAN S. (1962): A variational approach to the theory of the effective magnetic permeability of multiphase materials. J. Appl. Phys. 33, 3125–3131.

HERZOG P. (1956): Die Tektonik des Tafeljura und der Rheintalflexur südöstlich von Basel. Eclogae geol. Helv. 49, 317–362.

HORVÁTH F., BODRI L., OTTLIK P. (1979): Geothermics of Hungary and the tectonophysics of the Pannonian Basin 'Red Spot'. In: Čermák, V. & Rybach, L. (eds): Terrestrial Heat Flow in Europe, Springer. Heidelberg, 206–217.

HURTIG E., OELSNER, Ch. (1979): The heat flow field on the territory of the German Democratic Republic. In: Čermák, L. & Rybach L. (eds): Terrestrial Heat Flow in Europe. Springer, Heidelberg, 186–196.

JEFFREYS H. (1938): The disturbance of the temperature gradient in the earth's crust by inequalities of height, Monthly Not. Roy. Astr. Soc. Geophys. Suppl. 4. 309–312.

JOLY J. (1909): Radioactivity and Geology. Archibald Constable & Co., London, 287 p.

KAPPELMEYER O., HAENEL R. (1974): Geothermics. Geoexp. Monographs. Geopubl. Assoc., Bornträger, Berlin. 238 p.

KLINGELÉ E., OLIVIER R. (1980): La Nouvelle Carte Gravimétrique de la Suisse (Anomalies de Bouguer). Matériaux pour la Géologie de la Suisse, Géophysique no. 20, 93 p.

KÖNIGSBERGER J., THOMA E. (1906): Über die Beeinflussung der geothermischen Tiefenstufe durch Berge, Täler, Schichtstellung, durch fliessende Wässer und durch Wärme erzeugenden Einlagerungen. Eclogae geol. Helv. 9, 133–144.

KRÜSI H. R., BODMER Ph., RYBACH L. (1978a): Sammlung, Kompilation und Interpretation geothermischer Daten in der Schweiz, Schlussbericht an das BEW. 36 p.

KRÜSI H. R., BODMER Ph., RYBACH L. (1978b): Messung und Korrektur der Formationstemperaturen in der Erdölbohrung Treycovagnes 1, Bericht an das BEW. 25 p.

KUENZLI E. (1908): Temperatur- und Wasserverhältnisse im Weissensteintunnel. Beitr. Geol. Karte d. Schweiz, Sep. Dr., Neue Folge XX Lief. 126–143.

LACHENBRUCH A. H., BREWER M. C. (1959): Dissipation of the temperature effect in drilling a well in Arctic Alaska, Bull. U.S. Geol. Surv. 1083–C, 73–109.

LAMB H. H. (1971): Climates and circulation regimes developed over the northern hemisphere during and since the last ice age. Paleogeogr., -climatology, -ecology 10. 125–162.

LAPORTE M. (1962): Elaboration rapide des cartes gravimétriques déduites de l'anomalie de Bouguer à l'aide d'une calculatrice électronique. Geophys. Prosp. 10. 238–257.

LEGRAND R. (1975): Jalons geothermiques. Mem. Exp. Cartes géol. Min. Belg. 16, 44.

LODDO M., MONGELLI F. (1979): Heat Flow in Italy. In: Čermák, V. & Rybach, L. (eds.): Terrestrial Heat Flow in Europe. Springer, Heidelberg. 221–231.

NEFF (1980): Geothermische Prospektion im Raum Koblenz-Wildegg-Dielsdorf, Schlussbericht, Teil 1 des Forschungsprojektes "Geothermische Energie und unterirdische Wärmespeicherung", Nationaler Energie Forschungs Fonds, Basel. 162 p.

NEFF (1983a): Geothermisches Energiepotential des Felsgrundwasserträgers der Oberen Meeresmolasse im Blick auf Warmwassernutzung und Wärmespeicherung zwischen Reuss/Zugersee und Bodensee. Schlussbericht, Büro Dr. U. P. Büchi AG, Benglen.

NEFF (1983b): Energetische Bewirtschaftung des Untergrundes – Fallstudie Churer Rheintal. Schlussbericht, Tuffli & Partner AG Chur, Büchi & Müller AG Chur, Institut für Geophysik ETH Zürich.

OESCHGER H., MESSERLI B., SVILAR M. (1980): Das Klima. Geschichte und Zukunft. Springer, Heidelberg, 296 p.

PAVONI N. (1976): Isohypsenkarte des Grenzbereichs OMM/USM im Schweizer Alpenvorland. unpubl.

PIKA J. (1983): Zur Isotopengeochemie und Mineralogie der lacustrinen Ablagerungen im Zürichsee und im Schwarzen Meer. Mitg. Geol. Inst. ETH Zürich und Univ. Zürich, N. F. Nr. 243, 232 p.

RELLSTAB W. (1981): Der Einfluss des Paläoklimas auf das Temperaturfeld in der Schweiz, unpubl. interner Bericht, Institut für Geophysik ETH–Zürich, 63 p.

RELLSTAB W. (1982): dito. Ergänzung zum obengenannten Bericht, 8 p.

RYBACH L., WERNER D., MÜLLER St., BERSET G. (1977): Heat flow, heat production and crustal dynamics in the Central Alps, Switzerland. Techtonophysics 41, 113–126.

RYBACH L., FINCKH P. G. (1979a): Heat flow data in Switzerland. In: Čermák, V. & Rybach, L. (eds.): Terrestrial heat flow in Europe, Springer, Heidelberg, 278–282.

RYBACH L., BODMER Ph. (1980): Die geothermischen Verhältnisse der schweizerischen Geotraverse im Abschnitt Basel-Luzern. Eclogae geol. Helv. 73, 501–525.

RYBACH L., MÜLLER St., MILNES A. G., ANSORGE J., BERNOULLI D., FREY M. (1980): The Swiss Geotraverse Basel-Chiasso – a review. Eclogae geol. Helv. **73**, 437–462.

RYBACH L. (1981): Nutzungsmöglichkeiten geothermischer Energie in der Region Basel. Verhandl. Naturf. Ges. Basel **92**, 53–62.

RYBACH L., BODMER Ph., WEBER R., ENGLAND P. C. (1982): Heat flow and heat generation in the new Gotthard tunnel (Swiss Alps). In: Čermák, V. & Haenel, R. (eds.): Geothermics and Geothermal Energy. Schweizerbart, Stuttgart. 63–70.

RYBACH L., BODMER PH.(1983): Processing and representation of heat flow density maps – Part II: Construction and contouring of heat flow density maps. Zbl. Geol. Paläon. I, 87–92.

SADEE C. P. M. (1975): An interpretation of south Limburg subsurface temperature data. Geol. Mijnbouwh 54, 184–194.

SASS J. H., STONE C., MUNROE R. J. (1983): Thermal conductivity determination on solid rock – a comparison between a steady-state divided bar apparatus and a commercial transient line-source device. J. Volc. Geotherm. Res. 20. 145–153.

SCHÄRLI U. (1980): Methodische Grundlagen zur Erstellung eines Wärmeleitfähigkeitskataloges schweizerischer Gesteine. Diplomarbeit am Institut für Geophysik, ETH–Zürich. 126 p.

SCHÄRLI U. (1983): Petrophysikalische Daten von Gesteinen in der Schweiz. NEFF Interner Bericht 016. 24 p.

SCHÄRLI U., RYBACH L. (1984): On the thermal conductivity of low-porosity crystalline rocks. Tectonophysics 103. 307–313.

SCHWARZBACH M. (1961): Das Klima der Vorzeit. Enke, Stuttgart, 275 p.

STAPFF F. M. (1877): Studien über die Wärmevertheilung im Gotthard, I. Theil. 60. Jahresvers. Schweiz. Naturforsch. Ges. Bern.

STAPFF F. M. (1883): Some results of observations on underground temperature during the construction of the St. Gotthardtunnel. Proc. North Engl. Inst. Mech. Eng. 32, 14–34.

STEGENA L. (1976): The variation of temperature with depth in the Pannonian Basin. In: Ádám, A. (ed.): Geoelectric and Geothermal Studies. Akadémiai Kiadó, Budapest, 425–438.

SYNTHESE (1982): Geothermische Synthese der Schweiz. Eigd. Techn. Hochschule Zürich – Institut für Geophysik, Dr. U. P. Büchi Geol. Expertisen und Forschungen AG – Benglen ZH. Schriftenreihe des BEW Nr. 26, Bern, 61 p.

THIADENS A. A. (1968): The paleozoic of the Netherlands. Geol. Mijnbouwh. genotschap. Geol. Serv. 21–1, 9–28.

TRÜMPY R. (1980): Geology of Switzerland, A guide-book. Part A: An outline ofthe geology of Switzerland, Schweiz. Geolog. Kommission, Wepf & Co, Basel, 104 p.

VASSEUR G. (1982): Synthèse des résultats de flux géothermique en France. Annales de Géophysique 38, 189–201.

VON HERZEN R. P., UYEDA S. (1963): Heat flow through the Eastern Pacific floor. J. Geophys. Res. 69, 4234–4240.

WALSH J. B., DECKER, E. R. (1966): Effect of pressure and saturating fluid on the thermal conductivity of compact rock. J. Geophys. Res. 71, 3053–3061.

WENK H. R., WENK, E. (1969): Physical constants of Alpine rocks (Density, porosity, specific heat, thermal conductivity. Schweiz. Min. Petr. Mittg. 49, 343–368.

WERNER D., KÖPPEL V., HÄNNY R., RYBACH L. (1976): Cooling models for the Lepontine area (Central Swiss Alps). Schweiz. Min. Petr. Mitt. 56, 661–667.

WERNER D., FUCHS K. (1977): Evaluation and interpretation of the geothermal anomaly in the Rhine Graben. Int. Sem. on Geoth. Energy, CEC Bruxelles 1, 189–206.

WERNER D. (1981): A geothermal method for the reconstruction of the uplift history of a mountain range, applied to the Central Alps. Geol. Rundschau 70, 296–301.

ZOLLINGER A. (1925): Wärmeverteilung im Innern verschiedener Alpentunnels. Techn. Mitt. Eisenbahnwesen, Elektrotechnik, Bau- und Ingenieurwissenschaften, Zürich. Heft 1.

ZÜST O. (1977): Das Geländemodell des Informationsrasters. ORL. Disp. Nr.43, ETH–Zürich, 23–25.

Acknowledgments

We thank Prof. Dr. Stephan Mueller for continuous encouragement and support. We further obtained various help from many colleagues, especially from P. Angehrn (Degersheim), N. Balling (Aarhus), D. Blackwell (Dallas), U. Büchi (Forch), G. Buntebarth (Clausthal), A. Burger (Neuchâtel), V. Cermák (Prague), D. Chapman (Salt Lake City), J. Costain (Blacksburg), Y. Eckstein (Kent), Ph. England (Cambridge/Mass.), P. Finckh, R. Gable (Orléans), J. Goguel (Paris), R. Haenel (Hannover), L. Hauber (Basle), F. Horváth (Budapest), F. Jaffé (Geneva), E. Kissling, E. Klingelé, H. Laubscher (Basle), B. Mathey (Neuchâtel), J. Meunier (Strasbourg), F. Mongelli (Bari), P. Muffler (Menlo Park), E. Niggli (Berne), R. Oxburgh (Cambridge), N. Pavoni, H. Pollack (Ann Arbor), J. Sass (Phoenix), K. Sauer (Merzhausen), Hj. Schmassmann (Liestal), L. Stegena (Budapest), J. Toth (Edmonton), G. Vasseur (Montpellier), Th. Vollmayr (Hannover), D. Werner, and J. Wohlenberg (Aachen). Special thanks are due to J.-C-Griesser, H. R. Krüsi, W. Rellstab, R. Weber and U. Schärli for significant contributions. D. Galson critically read the manuscript and J. Dózsa prepared the majority of the figures.

Appendix 1: Drillhole objects, temperature data categories

Drillhole	Coordinates	Terrain elevation (m.a. sea level)	Depth (m)	Geology at bottom hole	Temperature data category						
					1	2	3	4	5	6	7
Allschwil 1	607980/267300	276	327	ma	×				×		
Allschwil 2	605960/265820	332	922	ma						×	×
Aqui, Zürich	682125/246569	419	500	omm			×		×		
Badenweiler 3 (D)	617225/294325	425	505	r	×		×		×		
Baitenhausen 1(D)	740300/286500	435	1500	ma						×	×
Balzers	757000/214000	480	620	dg				×			
Belmont Buss (F)	456019/292267	127	170	?							×
Bad Bellingen 3 (D)	608410/285980	225	1194	mm		×			×		
Berlingen	719685/280195	593	2311	r	×				×		
Besançon (F)	497061/233970	320	135	?						×	
KKW Beznau	659491/267242	326	322	mm				×			
Biaschina	709250/142050	455	653	kk				×			
Birmo AG	660350/257675	368	160	mm				×			
Bizonnes (F)	442667/40613	474	1424	?							×
Boswil	664845/237415	648	1836	ma	×				×		
Brislach	609175/253465	412	180	ma				×			
Bresse 2 (F)	413155/126691	190	1201	?							×
Bresse S1 (F)	422953/98601	287	2603	?							×
Bresse S2 (F)	431699/83527	314	1072	?							×
Bresse 103 (F)	407962/121297	216	1632	?							×
Bronschhofen	719500/260160	540	40	osm				×			
Brunnadern	728610/243300	680	60	osm				×	×		
Buggingen 1 (D)	613680/300650	222	830	ol						×	×
Buix	568780/258620	395	1053	?					×		×
Chapelle	547306/168360	764	1531	kr	×				×		
Chapéry (F)	491100/78000	600	4200	?	×				×		
Chiggiogna	706210/147380	700	305	kk					×		
Curciat (F)	424966/148568	197	530	?							×
Courtion	572415/189420	599	3084	mm	×				×		
Densbüren	646455/255054	516	237	mm				×			
Dingelsdorf 1 (D)	727950/288300	450	2702	gg						×	×
Dornbirn (A)	773523/256360	414	2820	usm	×					×	
Eclepens	533220/168380	527	2150	k		×			×		
Eglisau 2	680820/269865	380	423	ma	×				×		
Entlebuch	651250/202800	1080	5300	pk		×			×		
Essavilly (F)	495342/182123	792	2065	?							×
Essertines	539775/173490	661	2936	k				×			
Etrez (F)	426051/135567		1500	?							×
Ettenkirch 1 (D)	755800/286600	473	2161	ma							×
Faucigny (F)	516550/108950	766	4950	pk	×				×		
Feldkirch (F)	587300/300900	230	2103	dg				×			
Frenkendorf	621042/262365	308	300	mm				×			
Frick	644264/261903	346	297	mu						×	×
Furttal 709	ca.676000/256000	420	205	q				×			
Furttal 706	674350/255890	420	215	q				×			
Gossau Niederdorf	735200/252670	628	153	osm				×			
Gossau Silthang	738860/253180	700	31	osm				×			
Grellingen	610570/254310	326	213	dg				×			
Gubrist	677310/252755	585	200	osm				×			
Guspisbach (Schacht)	686800/161050	1691	520	kk					×		
Habsburg 5556.19	655150/256780	360	43	mo				×			
Hard 2 (A)	768600/263170	400	271	q					×		
Hartheim (D)	614200/310190	204	1143	ol						×	×
Heimersdorf (F)	583280/269090	392	798	dg			×		×		
Heitersheim (D)	613870/303370	216	1377	ol						×	×
Herdern	710308/274597	528	2154	mu ?		×			×		
Hirtzbach (F)	583250/272450	310	738	dg	×					×	
Hölzlisberg	757080/245780	570	194	dg				×			
Hospental	686800/164175	1364	300	kk				×			
Humilly 1 (F)	479200/105500	667	905	kr	×		×				
Humilly 2 (F)	480500/108250	504	3040	ka		×					
Hünenberg 1	675522/224593	461	3288	ma	×				×		
Jura 101 (F)	443880/133223	568	340	?							×
Kaiseraugst WB5	622630/264726	300	293	r					×		
Kaisten	644988/264509	353	70	mm					×		
Klingnau I	661356/271397	443	398	mu				×			
Klingnau II	661510/271750	420	282	mu				×			
Klingnau III	661830/271950	440	271	mu				×			
Knoeringue (F)	593470/268930	438	2149	gg	×				×		
Konstanz (D)	733250/284990	400	660	usm			×			×	
Kreuzlingen	729201/276169	538	2550	pk-gg	×				×		
Krozingen 3 (D)	618960/307710	225	610	mo				×	×		
Küsnacht	689296/241485	642	2693	ma	×				×		
Laufen	603510/250350	363	240	dg				×			
Lavin	804000/182460	1410	400	kk				×			
Leymen (F)	602840/261300	353	1155	dg				×			
Lindau	692815/255098	516	2377	gg	×				×		

Drillhole	Coordinates	Terrain elevation (m.a. sea level)	Depth (m)	Geology at bottom hole	Temperature data category						
					1	2	3	4	5	6	7
Linden	617704/188567	881	5448	k	×				×		
Bad Lostorf 3	637327/249242	549	584	mo					×		×
Malvallia	721870/142810	980	107	kk				×			
Martel Dernier	543730/203610	1025	300	kr				×			
Michelbach 101 (F)	575100/289950	348	1059	dg	×			×			
Moesrchwil	748180/258680	540	103	osm				×			
Mülligen BT2	659490/257200	355	74	mm				×			
Mumpf	636460/266270	282	207	r	×					×	
Neuwiller (F)	605800/263150	360	1063	dg		×					
Oberbueren	728740/257490	490	104	osm				×			
Oberdorf 92J1	623248/249274	506	125	mo				×			
Oberdorf 92J3	623720/249323	500	142	mm				×			
Oberhof Nord	642814/254407	550	62	mm				×			
Oberuzwil	728870/253400	640	40	osm				×			
Owingen (D)	729800/296700	523	1622	gg	×				×		
Pfaffnau 1	632708/231789	500	1843	gg	×				×		
Pfaffnau Süd 1	634950/228120	616	1209	ma	×				×		
Pfullendorf 3 (D)	735520/312440	654	1345	gg ?							×
Pratteln 41J7	618837/264121	276	100	mm				×			
Pratteln 41J8	620736/264539	271	127	mm				×			
Ratanelle (F)	414862/154430	183	1113	?							×
Riburg	629210/267200	300	210	mu				×			
Romanens	564200/167400	945	4022	k				×			
Ronchamp (F)	536551/285300		310	?							×
Rueras	700250/169750	1400	260	kk				×			
Ruppoldsried	599450/215600	483	996	ma				×			
Salève 2 (F)	495500/099300	812	1984	?	×					×	
Santa Maria	704350/160700	1823	1187	kk				×			
Savigny 1	546271/155312	839	2486	kr	×				×		
Schinznach 5256.26	652470/256730	460	61	mo?				×			
Schinznach QN83	653900/255430	350	25	q				×			
Servion	549000/157900	765	1433	usm							
Sevelen 13	755360/221900	460	38	q				×			
Sevelen 14	754840/222010	450	41	q				×			
Singen (D)	703990/286630	435	685	ma					×		×
Sorens	571900/168600	1019	3165	ma	×						
Soultz (F)	584435/301660	250	1830	?							×
Staffelfelden (F)	585300/297450	256	1918	dg	×					×	
Steinenstadt (D)	609130/289915	225	491	dg	×						
St. Germain (F)	481525/69368		450	?							×
Sundgau 201 (F)	589400/263100	448	582	dg	×					×	
Tiefenbrunnen/ZH	684200/245380	408	736	usm				×			
Thal Buechberg	759780/260260	470	55	omm				×			
Treycovagnes	536136/180273	474	3220	s		×			×		
Tschugg 1	572610/207910	463	704	ma				×			
Tuggen	714750/228760	408	1648	usm	×				×		
Vereina	793200/189250	1835	518	kk				×			
Vevy (F)	463436/98617	522	918	?							×
Wahlen	605670/249385	433	210	ma				×			
Walzenhausen	760880/256340	780	57	usm				×			
Weinstetten (D)	611980/306320	207	2404	mm	×					×	
Yverdon (Belair)	540724/180554	529	185	ol				×			
Zienken 1 (D)	611220/299380	223	1762	dg	×					×	
Zurzach 3	663742/271482	346	550	gg				×			
Zwingen	606905/253475	345	75	ma				×			

Explanation of symbols

Temperature data category:

1. uncorrected BHT
2. corrected BHT
3. Test temperature
4. Continuous temperature log
5. several temperature data
6. single temperature measurement
7. unknown temperature measurement method

Geology:

q	Quaternary	m	Muschelkalk
osm	Tertiary: "Upper Freshwater Molasse"		mo: upper
omm	Tertiary: "Upper Marine Molasse"		mm: middle
ol	Oligecene		mu: lower
usm	Tertiary: "Lower Freshwater Molasse"	s	Buntsandstein
e	Eocene	r	Rotliegendes
kr	Cretaceous	pk	Permocarboniferous
ma	Malm	ka	Carboniferous
dg	Dogger	gg	Crystalline basement
l	Liassic	kk	Crystalline rocks in the Alps

APPENDIX 2 : Thermal conductivities

SAMPLE	K(P)	K(S)	ANIS	S(P)	S(S)	GEOLOGY	LITHOLOGY
TSCHUGG 629.00	2.96	2.77	1.07	0.41	0.56	MARBRE BATARD	KALK,SAND.
TSCHUGG 640.30	4.21	3.85	1.09	0.18	0.62	PORTLAND	KALK,MERG.
TSCHUGG 642.10	4.59	4.38	1.05	0.10	0.30	PORTLAND	KALK
TSCHUGG 656.00	2.99	3.10	0.96	0.12	0.22	PORTLAND	KALK,BREKZ.
Z 1	3.40	5.27	0.64	0.36	0.72	OMM	SST
Z 2		3.49				OMM	SST
Z 4		3.22				OMM	SST
Z 5		4.49			0.34	OMM	SST
Z 6	3.21	2.63	1.22	0.17	0.14	OMM	SST
Z 11	4.74	5.19	0.91	1.05	1.22	OMM	SST
Z 12	3.33	3.75	0.89	0.47	0.80	OMM	SST
Z 14		4.01			0.14	OMM	SST
Z 17	3.10	5.17	0.60	0.12	0.39	OMM	SST,GRUNL.
Z 18	3.91	3.19	1.22	0.21	0.52	OMM	SST
Z 19	3.38	2.88	1.17	0.37	0.68	OMM	SST
Z 20	4.19	3.82	1.10	0.08	0.30	OMM	SST
Z 23	3.79	3.19	1.19	0.13	0.14	OMM	SST
BAECH 2		4.00			0.21	OMM	SST
GT 6		3.13				OMM	SST
GT 8		3.20				OMM	SST
GT 9	3.94	3.93	1.00	0.20	1.59	OMM	SST
GT 11		2.90				OMM	SST
UZ 1		3.04				USM	SST
UZ 2		2.45				USM	SST
UZ 4		3.29				USM	SST
B 1/11	2.50	2.36	1.06	0.05	0.08	USM	SST,GROB
B 4/3	3.16	3.09	1.02			USM	MGL
H 1/2	3.64	3.94	0.92			USM	SST
H 2/8	3.70	2.45	1.51	0.30	0.53	USM	SST,FEIN
H 2/10	2.96	2.14	1.38	0.04	0.12	USM	MGL,ROETL.
P 2/4	2.89	2.69	1.08			USM	SST,GROB
P 3/1	1.94	1.71	1.14	0.07	0.07	USM	SST
S 3/1	3.03	2.99	1.01			USM	MGL,ROETL.
S 3/3	3.31	3.15	1.05	0.06	0.42	USM	SST
GT 1	4.06	4.52	0.90	0.20	0.31	USM	SST

SAMPLE	K(P)	K(S)	ANIS	S(P)	S(S)	GEOLOGY	LITHOLOGY
GT 2		3.27				USM	SST
GT 3		1.02				USM	SST
GT 4		3.97			0.20	USM	SST
SM 27		2.78				USM	KALK POROES
SUE 26		2.74				USM	SUESSW.KALK
UBU 25		2.91				USM	KALK
UBU 18		3.24				USM	KALK
Z 7		3.13				USM	SST
Z 8		2.23				USM	SST
Z 9		2.92				USM	SST
Z 13		3.80			0.27	USM	SST
Z 16		2.07			0.42	USM	SST,GROB
Z 22		3.26			0.26	USM	SST
UR 19		3.36			0.09	URGON	KALK,POROES
URBL 28		2.47				URGONIAN	KALK
BA 23		3.35			0.05	BARREME,UNT.	KALK,MASSIG
PJ 30		3.12				HAUTERIVIAN	KALK POROES
HA 24		2.60				HAUTERIVIAN	KALK DICHT
PJ 24	2.58	2.89	0.89	0.44	0.79	HAUTERIVE	KALK,OOLITH.
VAL 20A	3.16	3.18	1.00	0.02	0.17	VALANGINIEN	KALK,OOIDE
MB 31		2.98				VALANGINE	CALCAIRE ROUX
P 21		2.44				PURBECKIAN	KALK SANDIG
POR 22		3.52			0.11	PORTLAND	KALK,DICHT
UPOR 32		2.74				U PORTLAND	KALK DICHT
KI 33		2.94				KIMMERIDGE	KALK DICHT
SE 31		2.54				SEQUANIAN	CALCAIRE ROUX
WE 58		2.45			0.06	WETTINGERSCH	KALK
WE 70		2.84			0.08	WETTINGERSCH	KALK
BA 67		2.51			0.05	BADENERSCH	KALK
WA 68		3.06			0.08	WANGENERSCH	KALK
WA 69		2.84			0.21	WANGENERSCH	KALK
WA 71		2.86			0.06	WANGENERSCH	KALK
WA 72		2.83			0.03	WANGENERSCH	KALK
WA 73		2.87			0.11	WANGENERSCH	KALK
WA 75		2.92			0.13	WANGENERSCH	KALK

SAMPLE	K(P)	K(S)	ANIS	S(P)	S(S)	GEOLOGY	LITHOLOGY
KKWB 25.50 M	1.92	1.36	1.41	0.13	0.14	OPALINUSTON	TON
KKWB 25.40 M	2.36	1.54	1.54	0.28	0.47	OPALINUSTON	TON
KKWB 28.80 M	2.27	1.35	1.68	0.04	0.09	OPALINUSTON	TON
KKWB 28.90 M	2.31	1.16	1.99	0.23	0.30	OPALINUSTON	TON
KKWB 30.24 M	2.71	2.24	1.21	0.03	0.26	OPALINUSTON	TON
KKWB 30.60 M	2.72	1.72	1.58	0.42	0.42	OPALINUSTON	TON
KKWB 32.40 M	2.53	1.93	1.32	0.07	0.15	OPALINUSTON	TON
KKWB 32.85 M	2.11	1.71	1.24	0.29	0.54	OPALINUSTON	TON
KKWB 37.20 M	2.21	1.22	1.81	0.19	0.15	OPALINUSTON	TON
KKWB 37.60 M	2.29	1.21	1.89	0.16	0.18	OPALINUSTON	TON
KKWB 37.70 M	2.30	1.71	1.34	0.38	0.54	OPALINUSTON	TON
KKWB 37.95 M	2.55	1.68	1.51	0.39	0.37	OPALINUSTON	TON
KKWB 38.10 M	2.31	1.22	1.88	0.19	0.18	OPALINUSTON	TON
KKWB 38.30 M	2.41	1.45	1.66	0.19	0.29	OPALINUSTON	TON
KKWB 42.68 M	2.34	1.50	1.56	0.07	0.13	OPALINUSTON	TON
KKWB 42.06 M	2.41	1.84	1.31	0.24	0.32	OPALINUSTON	TON
KKWB 42.65 M	2.18	1.43	1.53	0.20	0.31	OPALINUSTON	TON
KKWB 43.98 M	2.20	1.73	1.27	0.14	0.25	OPALINUSTON	TON
KKWB 46.20 M	2.49	1.22	2.04	0.14	0.17	OPALINUSTON	TON
KKWB 46.65 M	2.53	1.24	2.05	0.11	0.16	OPALINUSTON	TON
KKWB 49.80 M	2.52	1.16	2.17	0.04	0.12	OPALINUSTON	TON
KKWB 53.68 M	2.52	1.03	2.45	0.10	0.13	OPALINUSTON	TON
KKWB 56.95 M	2.25	1.15	1.96	0.27	0.30	OPALINUSTON	TON
KKWB 62.00 M	2.48	1.05	2.36	0.16	0.13	OPALINUSTON	TON
KKWB 65.60 M	2.36	1.25	1.89	0.15	0.25	OPALINUSTON	TON
KKWB 64.12 M	2.29	1.18	1.94	0.21	0.25	OPALINUSTON	TON
KKWB 66.25 M	2.08	2.11	.99	0.17	0.29	JURENSISSCH.	MERGEL,HART
KKWB 69.00 M	2.33	2.45	.95	0.17	0.41	JURENSISSCH.	KALK,MERGELIG
KKWB 69.58 M	1.91	1.61	1.18	0.13	0.32	POSIDONIENSCH.	KALKMERGEL
KKWB 70.87 M	1.92	1.47	1.31	0.05	0.23	POSIDONIENSCH.	MERGEL,TONIG
KKWB 74.20 M	1.43	.95	1.50	0.08	0.26	POSIDONIENSCH.	MERGEL,BITUM.
KKWB 74.60 M	2.73	2.91	.94	0.13	0.49	POSIDONIENSCH.	MERGEL,KALKIG
KKWB 76.16 M	2.30	2.54	.91	0.24	0.47	OBLIQUASCH.	KALK,MERGELIG
KKWB 77.50 M	2.14	1.61	1.33	0.10	0.39	OBTUSUSTONE	KALKMERGEL
KKWB 77.70 M	2.40	2.50	.96	0.08	0.23	OBTUSUSTONE	KALKMERGEL

SAMPLE	K(P)	K(S)	ANIS	S(P)	S(S)	GEOLOGY	LITHOLOGY
KKWB 79.04 M	2.74	2.35	1.17	0.05	0.42	OBTUSUSTONE	KALKMERGEL
KKWB 81.60 M	2.57	1.70	1.51	0.08	0.33	OBTUSUSTONE	MERGEL,SILT.
KKWB 82.00 M	2.67	1.63	1.64	0.14	0.17	OBTUSUSTONE	MERGEL,SILT
KKWB 84.80 M	2.52	1.63	1.54	0.21	0.37	OBTUSUSTONE	MERGEL,TONIG
KKWB 87.25 M	2.59	1.52	1.71	0.16	0.24	OBTUSUSTONE	MERGEL,TONIG
KKWB 90.97 M	2.07	1.79	1.16	0.13	0.26	ARIETENKALK	KALK,HART
KKWB 91.10 M	2.05	2.12	.97	0.05	0.17	ARIETENKALK	KALK,HART
KKWB 95.45 M	2.37	1.15	2.05	0.14	0.38	INSEKTENMERGEL	MERGEL,SILT.
KKWB 96.10 M	2.26	1.21	1.87	0.07	0.21	INSEKTENMERGEL	MERGEL,SILT.
KKWB 97.47 M	2.39	1.23	1.94	0.17	0.21	INSEKTENMERGEL	TON,SILT.
KKWB 97.90 M	2.27	1.10	2.07	0.20	0.18	INSEKTENMERGEL	TON,SILT.
KKWB 98.10 M	2.28	1.01	2.14	0.11	0.14	INSEKTENMERGEL	TON,SILT.
KKWB 98.70 M	2.05	2.14	.96	0.07	0.20	OB BUNTE MERGEL	MERGEL,DOLOM.
KKWB 98.90 M	2.31	2.14	1.08	0.23	0.53	OB BUNTE MERGEL	MERGEL,DOLOM.
KKWB 99.70 M	2.39	2.14	1.12	0.27	0.59	OB BUNTE MERGEL	MERGEL,DOLOM.
KKWB100.70 M	2.29	2.29	1.00	0.22	0.48	OB BUNTE MERGEL	MERGEL,DOLOM.
KKWB100.70 M	2.29	2.29	1.00	0.22	0.48	OB BUNTE MERGEL	MERGEL,DOLOM.
RUPP. 383.90	3.34	2.58	1.29			USM	SST
RUPP. 646.00	3.41	2.57	1.33	0.05	0.10	USM	TON
RUPP. 668.30	2.82	2.82	1.00	0.02	0.50	USM	SST
RUPP. 733.00	3.23	3.09	1.04			USM	SILT,MERG.
RUPP. 733.00	3.23	2.51	1.29			USM	SILT,MERG.
RUPP. 773.10	2.78	3.47	0.80	0.16	0.32	USM	SST
RUPP. 815.30	3.49	2.73	1.28	0.04	0.25	USM	SST
RUPP. 875.50	2.58	1.97	1.31	0.04	0.05	UMM	KALK
RUPP. 890.50		3.51			0.21	PORTLAND	KALK,TONH.
RUPP. 946.80		3.58			0.19	PORTLAND	KALK,TONH.
RUPP. 950.90	3.43	3.46	0.99	0.15	0.51	PORTLAND	KALK,MERG.
TSCHUGG 422.00	2.56	2.87	0.89			USM	SST
TSCHUGG 513.00		3.15			0.41	URGON (BLANC)	
TSCHUGG 516.30	3.51	3.17	1.11	0.08	0.35	URGON (BLANC)	KALK,MERG.
TSCHUGG 533.80	3.36	3.64	0.92	0.11	0.26	URGON (JAUNE)	MGL,KALK.
TSCHUGG 596.50	3.05	3.03	1.01			VALANGIEN	MGL,DRUSIG
TSCHUGG 602.40	3.66	3.16	1.16	0.03	0.22	MARBRE BARARD	
TSCHUGG 608.50		3.33			0.34	MARBRE BATARD	KALK,TONH.

SAMPLE	K(P)	K(S)	ANIS	S(P)	S(S)	GEOLOGY	LITHOLOGY
GE 65		2.75			0.22	GEISSBERGSCH	KALK
GE 66		2.82			0.17	GEISSBERGSCH	KALK
GE 74		2.66			0.07	GEISSBERGSCH	KALK
EFF 59		2.66			0.10	EFFINGERSCH	MERGEL
EFF 60		2.07			0.07	EFFINGERSCH	MERGEL
EFF 64		1.96			0.05	EFFINGERSCH	MERGEL
O 41		2.51				EFFINGERSCH	OXF.MERGELK.
OX 40		2.29				BIRMENSDSCH	KALK DICHT
CCR 37		2.55				CALLOVIAN	CALC.ROUX SAB
DN 41		2.85				CALLOVIAN	ECHIN.BRECCIE
DN 38		2.92				CALLOVIAN	ECHIN.KALK
OHR 36		2.77				O HAUPTROGENST.	OOLITH,KALK
HR 51		2.84			0.1	HAUPTROGENST	KALK,MASSIG
HR 52		3.03			0.18	HAUPTROGENST	MASSIGER KALK
HR 53		2.95			0.10	HAUPTROGENSTEIN	KALK,MASSIG
HR 54		2.76			0.15	HAUPTR.STEIN	KALK
UHR 35		2.42				U HAUPTROGENST.	OOLITH,KALK
MBL 39		2.86				MARNES BLANCHES	MERGELKALK
CCE 42		2.78				CALC.A ENTROQU.	KALK MASSIG
MU 50		2.46			0.06	MURCHISONSCH	EISENH.KALK
O 1		1.38				OPALINUSTON	MERGEL
OBL 3		2.63				OBLIQUASCH	KALK
ML 2		2.41				M LIAS	KALK
RHAE 10		2.41				O KEUPER	SST ROT
DOL 10		3.29				OB BUNTE MERGEL	DOLOMIT FEIN
OBU 4	4.05	5.81	0.70	0.23	0.55		KALK,MERG.
GA 5		3.96				GANSINGERDOLO	DOLOMIT
SS 13		1.92				SCHILFSST	SST ROETL.
SCHI 1	2.85	2.74	1.04			SCHILFSANDSTEIN	SST
G 14		0.98				GIPSKEUPER	GIPS DICHT
KEU 7		4.03			0.40	GIPSKEUPER	DOLOMIT
TR 15		3.58				TROCHITENKALK	KALK POROES
GK 12		2.80				GIPSKEUPER	GIPS POROES
GK 12		4.14				GIPSKEUPER	GIPS POROES
TRI 6		3.77				TRIGONODUSDOLO	DOLOMIT

SAMPLE	K(P)	K(S)	ANIS	S(P)	S(S)	GEOLOGY	LITHOLOGY
AN 16A		3.23				SULFATZONE	KALK POROES
AN 16B		3.23				DOLOMITZONE	DOLOMIT
M 2	2.72			0.11		BUNTSANDSTEIN	SST
M 3	2.52			0.36		BUNTSANDSTEIN	SST
M 5A	2.75			0.46		BUNTSANDSTEIN	SST
M 5B	4.47			0.43		BUNTSANDSTEIN	KGL.
M 6	2.77			0.46		BUNTSANDSTEIN	SST
M 8	4.54			0.67		BUNTSANDSTEIN	SST
M 10	5.10			0.50		BUNTSANDSTEIN	SST
M 11	4.51			0.58		BUNTSANDSTEIN	SST
M 12	2.64			0.36		BUNTSANDSTEIN	SST
M 12A	4.23			0.79		BUNTSANDSTEIN	KGL.
M 14	6.63			0.27		BUNTSANDSTEIN	SST
M 15	5.82			0.65		BUNTSANDSTEIN	SST
M 17	3.04			0.70		BUNTSANDSTEIN	SST
QP 85	2.86	2.60	1.10	0.09	0.23	KRISTALLIN	QUARZPORPH.
HG 74A 608.50	3.99	3.90	1.02	0.04	0.46	KRISTALLIN	MONZOGRANIT
L 79A G 608.50		2.23			0.09	KRISTALLIN	KERSANTIT
NO 58B	3.64	3.62	1.00	0.14	0.42	KRISTALLIN	GRANODIORIT

LEGEND

All thermal conductivities are in W/m,^{o}K

K(P) = thermal conductivity parallel to layering/schistosity

K(S) = thermal conductivity perpendicular to layering/schistosity

ANIS = anisotropy of thermal conductivity = K(P)/K(S)

S(P) = standard deviation of K(P)

S(S) = standard deviation of K(S)

APPENDIX 3
HEAT FLOW DENSITY (MILLIWATT/SQ.METER)

CORRECTED FOR TOPOGRAPHY

SWISS COORDINATES		SITE	GEOGRAPHIC COORDINATES		ZMIN	ZMAX	H	NT	NK	HFD	DHFD
607980.	267300.	ALLSCHWIL 1	47334N	7327E	0.	327.	280.	5	5	94.	68.
502134.	80113.	ANNECY	45520N	6107E	0.	0.	0.	0	0	111.	0.
505920.	72642.	ANNECY	45480N	6137E	0.	0.	0.	0	0	68.	0.
608410.	285980.	BAD BELLINGEN	47435N	7331E	0.	1100.	230.	2	17	135.	-1.
740300.	256500.	BAITENHAUSEN	47267N	9180E	0.	1500.	0.	4	3	105.	14.
662597.	227543.	BALDEGGERSEE	47118N	8159E	0.	0.	0.	0	0	96.	0.
757000.	214000.	BALZERS	47035N	9303E	27.	600.	480.	125	2	78.	3.
456019.	292267.	BELMONT BUSS (F)	47459N	5311E	50.	127.	0.	0	1	150.	0.
719685.	280195.	BERLINGEN 1	47397N	9019E	0.	2312.	590.	3	16	91.	-1.
497061.	233970.	BESANÇON TH(F)	47149N	6047E	90.	135.	0.	0	1	74.	0.
659490.	267240.	BEZNAU	47332N	8138E	0.	300.	330.	27	22	106.	7.
709250.	142050.	BIASCHINA	46253N	8516E	0.	640.	460.	103	7	79.	1.
580380.	218291.	BIELERSEE	47069N	7108E	0.	0.	0.	0	0	59.	0.
660350.	257700.	BIRMO AG	47281N	8146E	0.	79.	370.	22	4	155.	13.
442667.	40613.	BIZONNES (F)	45300N	5256E	0.	1424.	0.	0	3	96.	0.
749471.	273872.	BODENSEE	47359N	9256E	0.	0.	0.	0	0	116.	0.
747019.	275662.	BODENSEE	47369N	9237E	0.	0.	0.	0	0	115.	0.
743215.	277422.	BODENSEE	47379N	9207E	0.	0.	0.	0	0	122.	0.
748441.	262726.	BODENSEE	47299N	9246E	0.	0.	0.	0	0	117.	0.
664850.	237420.	BOSWIL 1	47171N	8178E	0.	1836.	650.	1	5	70.	0.
478941.	67567.	BOURGET	45450N	5530E	0.	0.	0.	0	0	68.	0.
478960.	69419.	BOURGET	45460N	5530E	0.	0.	0.	0	0	65.	0.
614687.	299990.	BRD	47511N	7381E	0.	0.	0.	0	0	70.	0.
413155.	126691.	BRESSE 2 (F)	46160N	5009E	894.	1201.	0.	0	3	98.	0.
422953.	98601.	BRESSE S1 (F)	46010N	5091E	0.	2603.	0.	0	0	96.	0.
431699.	83527.	BRESSE S2 (F)	45530N	5162E	0.	1072.	0.	0	0	113.	0.
407962.	121297.	BRESSE 103 (F)	46130N	4570E	0.	1632.	0.	0	0	108.	0.
719500.	260160.	BRONSCHHOFEN TRUENGE	47289N	9015E	15.	40.	540.	26	2	97.	10.
728610.	243300.	BRUNNADERN	47197N	9084E	12.	56.	680.	45	1	34.	2.
568920.	258760.	BUIX	47288N	7016E	0.	888.	400.	24	12	109.	4.
547310.	168360.	CHAPELLE	46399N	6450E	0.	1500.	760.	2	6	92.	-1.
706210.	147380.	CHIGGIOGNA	46282N	8493E	0.	305.	700.	56	1	49.	5.
731436.	86312.	COMERSEE	45550N	9080E	0.	0.	0.	0	0	75.	0.
731436.	86312.	COMERSEE	45550N	9080E	0.	0.	0.	0	0	71.	0.
741549.	97659.	COMERSEE	46010N	9160E	0.	0.	0.	0	0	103.	0.
424966.	148508.	COURCIAT DONG (F)	46280N	5096E	0.	1530.	0.	0	0	100.	0.
572415.	189420.	COURTION	46513N	7046E	0.	3077.	0.	2	25	69.	-1.
728200.	285900.	DINGELSDORF (BRD)	47427N	9088E	0.	1046.	450.	2	2	83.	0.
773523.	256300.	DORNBIRN (OE)	47261N	9444E	0.	2820.	430.	2	1	115.	0.
533220.	168380.	ECLEPENS	46398N	6340E	0.	2142.	530.	3	5	86.	-1.
680800.	269880.	EGLISAU 2	47345N	8308E	0.	423.	380.	2	6	102.	-1.
651250.	202800.	ENTLEBUCH	46585N	8067E	0.	5230.	1080.	6	5	88.	23.
495342.	182123.	ESSAVILLY (F)	46470N	6041E	1828.	2065.	0.	0	2	61.	0.
539780.	173490.	ESSERTINES	46426N	6391E	0.	3000.	660.	30	19	104.	4.
426051.	135567.	ETREZ (F)	46210N	5107E	1400.	1500.	0.	0	4	102.	0.
750630.	280600.	ETTENKIRCH	47396N	9267E	0.	3000.	470.	30	7	82.	7.
516550.	117950.	FAUCIGNY	46125N	6214E	0.	0.	0.	0	0	82.	0.
586948.	299801.	FELDKIRCH(F)	47510N	7159E	600.	1600.	0.	0	0	86.	0.
621040.	262370.	FRENKENDORF	47307N	7431E	0.	235.	310.	39	14	164.	8.
676830.	153740.	FURKA	46319N	8264E	0.	1460.	2950.	18	2	28.	7.
674350.	255890.	FURTTAL 706	47270N	8255E	0.	205.	420.	37	2	64.	3.
676000.	256000.	FURTTAL 709	47271N	8268E	0.	175.	420.	34	2	95.	8.
852318.	64232.	GARDASEE	45410N	10407E	0.	0.	0.	0	0	117.	0.
853522.	67969.	GARDASEE	45430N	10417E	0.	0.	0.	0	0	120.	0.
735200.	252670.	GOSSAU NIDERDORFER F	47247N	9138E	0.	153.	630.	75	3	134.	13.
738860.	253180.	GOSSAU SILTHANG N1	47249N	9168E	21.	31.	700.	11	2	187.	34.
689090.	156200.	GOTTHARD SBB 3	46331N	8360E	0.	1250.	2400.	22	2	50.	4.
688380.	164400.	SBB GOTTHARDTUNNEL 1	46375N	8356E	0.	720.	1840.	21	2	51.	10.
686630.	159480.	GOTTHARD 2	46349N	8341E	0.	1200.	2370.	18	2	60.	8.
686690.	159290.	GOTTHARD 2	46348N	8342E	0.	1240.	2410.	24	2	43.	9.
687510.	166480.	GOTTHARDSTRASSENTUNN	46387N	8349E	0.	690.	1810.	20	3	69.	6.
693040.	246150.	GREIFENSEE	47216N	8402E	0.	0.	0.	0	0	109.	0.
694120.	244941.	GREIFENSEE	47209N	8411E	0.	0.	0.	0	0	110.	0.
610570.	254310.	GRELLINGEN	47264N	7347E	12.	210.	330.	43	7	80.	10.
677310.	252780.	GUBRIST	47253N	8278E	0.	180.	590.	24	2	135.	3.
686230.	161050.	GUSPISBACH	46357N	8339E	0.	519.	1690.	29	1	86.	4.
655150.	256780.	HABSBURG 5556.19	47276N	8102E	0.	43.	360.	22	1	184.	37.
768600.	263170.	HARD 2	47299N	9406E	193.	271.	400.	3	2	68.	23.
585700.	269000.	HEIMERSDORF	47343N	7149E	0.	798.	360.	5	7	110.	65.
710300.	274600.	HERDERN	47368N	8544E	0.	2154.	520.	50	14	104.	3.
757080.	245760.	HOELZLISBERG	47207N	9311E	20.	194.	570.	175	1	50.	1.
675520.	224590.	HUENENBERG 1	47101N	8261E	0.	3288.	460.	4	5	65.	15.
492135.	108075.	HUMILLY 2 (F)	46070N	6026E	1998.	2926.	0.	0	3	51.	0.
802230.	66044.	ISEOSEE	45430N	10022E	0.	0.	0.	0	0	120.	0.
802199.	67896.	ISEOSEE	45440N	10022E	0.	0.	0.	0	0	94.	0.
443880.	133223.	JURA 101 (F)	46200N	5246E	0.	340.	0.	0	0	83.	0.
622500.	265100.	KAISERAUGST	47322N	7443E	0.	293.	300.	4	16	69.	64.
661460.	271500.	KLINGNAU I	47355N	8154E	0.	367.	440.	34	21	118.	12.
661510.	271750.	KLINGNAU II	47356N	8154E	0.	282.	420.	12	1	111.	18.

APPENDIX 3
HEAT FLOW DENSITY (MILLIWATT/SQ.METER)

CORRECTED FOR TOPOGRAPHY

SWISS COORDINATES		SITE	GEOGRAPHIC COORDINATES		ZMIN	ZMAX	H	NT	NK	HFD	DHFD
661830.	271950.	KLINGNAU III	47358N	8157E	0.	271.	440.	15	1	148.	22.
593120.	268780.	KNOERINGUE	47342N	7208E	0.	2152.	440.	5	15	74.	-1.
729200.	276170.	KREUZLINGEN	47374N	9095E	0.	2547.	540.	3	16	98.	-1.
689296.	241485.	KUESNACHT	47191N	8372E	0.	2682.	0.	2	5	69.	-1.
804000.	182400.	LAVIN	46458N	10066E	78.	333.	1410.	28	1	46.	3.
537072.	144486.	LEMAN	46270N	6372E	0.	0.	0.	0	0	86.	0.
533249.	144528.	LEMAN	46270N	6342E	0.	0.	0.	0	0	79.	0.
525591.	142766.	LEMAN	46260N	6282E	0.	0.	0.	0	0	92.	0.
602051.	260873.	LEYMEN(F)	47299N	7280E	150.	220.	0.	0	3	70.	0.
692815.	255098.	LINDAU	47264N	8402E	0.	2376.	0.	6	17	109.	23.
617704.	188567.	LINDEN	46509N	7403E	0.	5437.	890.	7	11	70.	20.
637330.	249240.	LOSTORF	47236N	7560E	0.	550.	550.	3	26	96.	9.
621800.	140930.	LOETSCHBERG	46252N	7433E	0.	1540.	2780.	65	1	62.	2.
721729.	96298.	LAGO DI LUGANO	46005N	9006E	0.	0.	0.	0	0	91.	0.
716256.	88778.	LAGO DI LUGANO	45565N	8563E	0.	0.	0.	0	0	94.	0.
712000.	87462.	LAGO DI LUGANO	45558N	8530E	0.	0.	0.	0	0	111.	0.
712758.	90546.	LAGO DI LUGANO	45574N	8536E	0.	0.	0.	0	0	93.	0.
722785.	97246.	LAGO DI LUGANO	46010N	9015E	0.	0.	0.	0	0	91.	0.
692975.	91152.	MAGGIORE	45580N	8383E	0.	0.	0.	0	0	124.	0.
695505.	94897.	MAGGIORE	46000N	8403E	0.	0.	0.	0	0	131.	0.
721870.	142810.	MALVALLIA	46256N	9015E	0.	107.	980.	76	3	57.	10.
543730.	203610.	MARTEL DERNIER	46589N	6419E	0.	300.	1030.	14	1	60.	9.
557226.	77662.	MONT BLANC	45510N	6533E	0.	0.	0.	0	0	83.	0.
748180.	258680.	MOERSCHWIL STEINACH	47278N	9243E	0.	103.	540.	92	2	100.	3.
659490.	257200.	BTZ MUELLIGEN	47278N	8137E	55.	71.	360.	8	4	179.	61.
558929.	199874.	NEUCHATELLERSEE	46570N	6540E	0.	0.	0.	0	0	76.	0.
553834.	194353.	NEUCHATELLERSEE	46539N	6500E	0.	0.	0.	0	0	78.	0.
728740.	257490.	OBERBUEREN SONNENTAL	47274N	9088E	0.	104.	490.	105	2	93.	9.
728870.	253400.	OBERUZWIL BICHWIL	47252N	9088E	0.	40.	640.	40	2	85.	13.
729300.	296700.	OWINGEN	47485N	9103E	0.	1622.	520.	3	4	103.	4.
692830.	124050.	PALAGNEDRA 3	46157N	8386E	0.	1270.	1770.	17	2	80.	22.
692460.	114920.	PALAGNEDRA 1	46108N	8382E	0.	790.	1270.	13	2	48.	21.
632710.	231790.	PFAFFNAU	47142N	7522E	0.	1814.	500.	3	19	91.	-1.
735520.	312440.	PFULLENDORF (BRD)	47569N	9152E	0.	1500.	650.	6	15	126.	14.
620740.	264540.	PRATTELN 4138	47319N	7429E	0.	125.	270.	25	9	81.	7.
414862.	154430.	RATANELLE 101 (F)	46310N	5015E	622.	1113.	0.	0	3	121.	0.
629210.	267200.	RIBURG NR 2	47333N	7496E	0.	210.	300.	168	12	74.	3.
594200.	167400.	ROMANENS	46395N	7218E	0.	3820.	0.	3	10	86.	42.
536551.	285300.	RONCHAMP(F)	47429N	6356E	100.	310.	0.	0	7	108.	0.
700250.	169750.	RUERAS	46403N	8449E	75.	260.	1400.	19	1	72.	6.
599450.	215600.	RUPPOLDSRIED	47055N	7259E	0.	934.	480.	44	7	93.	2.
503565.	98617.	SALEVE (F)	46020N	6116E	0.	1984.	0.	0	0	58.	0.
481525.	69368.	ST GERMAIN(F)	45460N	5549E	100.	450.	0.	0	0	46.	0.
704350.	160700.	STA. MARIA	46354N	8480E	0.	1187.	1190.	29	1	56.	4.
546270.	155310.	SAVIGNY 1	46328N	6443E	0.	2319.	840.	3	6	86.	15.
653900.	255430.	SCHINZNACH QN 83	47269N	8092E	0.	25.	350.	18	2	91.	26.
652470.	256730.	SCHINZNACH 5256.26	47276N	8081E	0.	61.	460.	21	2	90.	15.
754840.	222010.	SEVELEN 14	47079N	9288E	31.	71.	450.	41	2	69.	3.
755360.	221900.	SEVELEN 13	47078N	9292E	35.	73.	460.	38	4	46.	1.
651810.	123610.	SIMPLON S	46157N	8066E	0.	1710.	2420.	20	4	48.	6.
650660.	124600.	SIMPLON N	46163N	8058E	0.	2120.	2820.	54	2	75.	6.
703990.	286630.	SINGEN (BRD)	47434N	8495E	0.	5000.	440.	13	5	64.	5.
584435.	301660.	SOULTZ (F)	47519N	7138E	1824.	1830.	0.	0	2	109.	0.
759780.	260260.	THAL BUECHBERG	47285N	9335E	10.	55.	470.	46	2	62.	7.
684200.	245350.	TIEFENBRUNNEN	47212N	8332E	145.	722.	410.	86	5	97.	3.
536140.	180280.	TREYCOVAGNES 1	46463N	6362E	0.	3210.	470.	5	16	85.	27.
572610.	207910.	TSCHUGG	47013N	7047E	0.	481.	0.	27	15	105.	2.
714750.	228760.	TUGGEN	47120N	8572E	0.	1300.	410.	6	3	102.	7.
694550.	112510.	VERBANO 2	46095N	8398E	0.	480.	910.	16	2	28.	17.
696870.	111410.	VERBANO 1	46089N	8416E	0.	850.	1280.	12	2	48.	11.
793200.	189250.	VEREINA	46496N	9583E	0.	485.	1840.	26	1	49.	3.
463436.	98617.	VEVY	46015N	5405E	0.	918.	0.	0	0	125.	0.
675591.	207622.	VIERWALDSTAETTERSEE	47009N	8260E	0.	0.	0.	0	0	122.	0.
679419.	203966.	VIERWALDSTAETTERSEE	46589N	8290E	0.	0.	0.	0	0	120.	0.
681955.	204001.	VIERWALDSTAETTERSEE	46590N	8310E	0.	0.	0.	0	0	109.	0.
760880.	256340.	WALZENHAUSEN HERHOL	47263N	9343E	10.	57.	780.	48	2	70.	5.
680599.	216951.	ZUGERSEE	47059N	8300E	0.	0.	0.	0	0	115.	0.
680599.	216951.	ZUGERSEE	47059N	8300E	0.	0.	0.	0	0	123.	0.
688063.	235585.	ZUERICHSEE	47159N	8362E	0.	0.	0.	0	0	118.	0.
688063.	235585.	ZUERICHSEE	47159N	8362E	0.	0.	0.	0	0	125.	0.
663970.	271220.	ZURZACH NR 3	47353N	8174E	15.	695.	340.	346	15	126.	2.

LEGEND
ZMIN : MINIMUM DEPTH FOR HFD EVALUATION (M)
ZMAX : MAXIMUM DEPTH FOR HFD EVALUATION (M)
H : ELEVATION OF SITE (M)
NT : NUMBER OF TEMPERATURE MEASUREMENTS
NK : NUMBER OF CONDUCTIVITY VALUES USED FOR HFD DETERMINATION
HFD : HEAT FLOW DENSITY (MILLIWATT/SQ.METER)
DHFD : UNCERTAINITY OF THE HFD DETERMINATION (MILLIWATT/SQ.METER)
-1 : REGRESSION (BULLARD PLOT) NOT SIGNIFICANT

Achevé d'imprimer sur les presses
de l'Imprimerie Paul Attinger SA, à Neuchâtel
en 1984

Contributions to the Geology of Switzerland
Beiträge zur Geologie der Schweiz
Matériaux pour la Géologie de la Suisse

Geophysics – Geophysik – Géophysique

No.		Fr.
1	**H. Röthlisberger.** Zur seismischen und petrographischen Charakterisierung einiger Molassegesteine, einschliesslich der Beschreibung von Methoden der Korngrössenbestimmung in Festmaterial. 91 Seiten, 31 Figuren. 1957	14.–
2	**O. Friedenreich.** Eine grossräumige Widerstandskartierung nordwestlich von Zürich und ihre geologische Deutung. 47 Seiten, 22 Textfiguren, 9 Karten. 1959	20.–
3	**F. Gassmann.** *Schweremessungen in der Umgebung von Zürich. 70 Seiten, 24 Textfiguren, 2 Tafeln. 1962*	24.–
4	**E. Poldini.** Les Anomalies gravifiques du canton de Genève. Avec 63 pages, 25 figures et 3 planches. 1963	24.–
5	**L. Rybach.** Refraktionsseismische Untersuchungen im Raum Aare-, Limmat- und Surbtal. 49 Seiten, 42 Figuren. 1962	14.–
6	**O. Gonet.** Etude gravimétrique de la plaine du Rhône. Région Saint-Maurice – Lac Léman. 50 pages, 30 figures, 2 planches. 1965	14.–
7	**C. Meyer de Stadelhofen.** Carte des résistivités de la plaine du Rhône. 8 pages, 2 figures, 2 planches. 1966	8.–
8	**O. Gonet.** Etude gravimétrique du lac Léman à bord du mésoscaphe *Auguste Picard.* 20 pages, 8 figures, 1 planche. 1969	8.–
9	**J.-J. Wagner.** Elaboration d'une carte d'anomalie de Bouguer. Etude de la vallée du Rhône de Saint-Maurice à Saxon (Suisse). 91 pages, 32 figures, 2 planches. 1970	22.–
10	**H. Lazreg.** Etude géophysique, géologique et hydrogéologique de la région de Concise à Pompaples (pied du Jura vaudois). 51 pages, 16 figures, 7 planches. 1971	22.–
11	**M. Petch.** Contribution à l'étude hydrogéologique de la plaine de l'Orbe. 95 pages, 23 figures, 15 planches. 1970	22.–
12	**P.-A. Gilliand.** Etude géoélectrique du Klettgau (Suisse), canton de Schaffhouse. 85 pages, 47 figures, 10 annexes, 5 planches. 1970	22.–
13	**P. Corniche.** Application des méthodes géophysiques à la recherche hydrogéologique. 65 pages, 25 figures. 1973	22.–
14	**F. Heller.** Magnetische und petrographische Eigenschaften der granitischen Gesteine des Albignagebietes (Nördliches Bergeller Massiv). 66 Seiten, 24 Textfiguren. 1972	22.–
15	**E. Klingelé.** Contribution à l'étude gravimétrique de la Suisse romande et des régions avoisinantes. 94 pages, 6 figures, 35 planches. 1972	22.–
16	**W. Sigrist.** Contribution à l'étude géophysique des fonds du lac Léman. 56 pages, 28 figures, 1 planche. 1974	22.–
17	**R. Olivier.** Elaboration d'un système de traitement gravimétrique géré par l'ordinateur. Etude gravimétrique du plateau romand de Versoix (GE) à Concise (VD). 56 pages, 21 figures, 10 planches. 1974	22.–
18	**H. Buchli, R. Paquin, A. Donzé.** Etude géoélectrique et gravimétrique du Chablais entre Asnières et Evian. 170 pages, 81 figures, 4 planches. 1976	32.–
19	**G. Fischer, P.-A. Schnegg, J. Sesiano.** A new geomagnetic survey of Switzerland. 44 pages, 15 figures, 8 tables, 10 cartes. 1979	28.–
20	**E. Klingelé, R. Olivier.** La nouvelle carte gravimétrique de la Suisse (Anomalies de Bouguer). 96 pages, 9 figures, 4 tables, 1 carte. 1980	28.–
21	**J.-J. Wagner, St. Mueller.** Geomagnetic and gravimetric studies of the Ivrea zone. 64 pages, 44 figures. 1984	32.–
22	**Ph. Bodmer, L. Rybach.** Geothermal map of Switzerland (Heat flow density). 48 pages, 21 figures, 6 tables. 1984	36.–

Kommissionsverlag - En Commission chez
Kümmerly & Frey, Geographischer Verlag, Bern